SARS-CoV-2 infection of human pluripotent stem cell-derived vascular cells reveals smooth muscle cells as key mediators of vascular pathology during infection

Alexsia Richards[1#], Andrew Khalil[1,2,3#], Max Friesen[1], Troy W. Whitfield[1], Tenzin Lungjangwa[1], Lee Gehrke[4,5,6], David Mooney[3,4,*], Rudolf Jaenisch[1,6, 7*]

[1]Whitehead Institute for Biomedical Research, Cambridge, Massachusetts, 02127
[2]Wyss Institute for Biologically Inspired Engineering, Harvard University, Boston, MA 02115
[3]John A. Paulson School of Engineering and Applied Sciences, Harvard University, Cambridge, Massachusetts, 02138
[4]Department of Microbiology, Harvard Medical School, Boston, MA 02115
[5] Institute for Medical Engineering and Science, Massachusetts Institute of Technology, Cambridge, Massachusetts, 02127
[6]Department of Biology, Massachusetts Institute of Technology, Cambridge, Massachusetts, 02127
[7] Lead Contact
[#] Equal author contributions
*Correspondence: mooney@seas.harvard.edu, jaenisch@wi.mit.edu

Summary

Although respiratory symptoms are the most prevalent disease manifestation of infection by Severe Acute Respiratory Syndrome Coronavirus 2 (SARS-CoV-2), nearly 20% of hospitalized patients are at risk for thromboembolic events[1]. This prothrombotic state is considered a key factor in the increased risk of stroke, which has been observed clinically during both acute infection and long after symptoms have cleared[2]. Here we developed a model of SARS-CoV-2 infection using human-induced pluripotent stem cell-derived endothelial cells, pericytes, and smooth muscle cells to recapitulate the vascular pathology associated with SARS-CoV-2 exposure. Our results demonstrate that perivascular cells, particularly smooth muscle cells (SMCs), are a specifically susceptible vascular target for SARS-CoV-2 infection. Utilizing RNA sequencing, we characterized the transcriptomic changes accompanying SARS-CoV-2 infection of SMCs, and endothelial cells (ECs). We observed that infected human SMCs shift to a pro-inflammatory state and increase the expression of key mediators of the coagulation cascade. Further, we showed human ECs exposed to the secretome of infected SMCs produce hemostatic factors that can contribute to vascular dysfunction, despite not being susceptible to direct infection. The findings here recapitulate observations from patient sera in human COVID-19 patients and provide mechanistic insight into the unique vascular implications of SARS-CoV-2 infection at a cellular level.

Introduction

Over the past 20 years, human coronaviruses have been responsible for severe outbreaks worldwide, including the Severe Acute Respiratory Syndrome (SARS) outbreak of 2003 and the Middle East Respiratory Syndrome (MERS) outbreak of 2012[3]. Most recently, the global pandemic caused by the Severe Acute Respiratory Syndrome Coronavirus 2 (SARS-CoV-2) has led to over 700 million documented cases and nearly 7 million deaths as of January 2023[4]. Although the primary symptoms of SARS-CoV-2 infection are associated with the respiratory system, severe illness is also associated with devastating vascular complications[5]. Most notable of these complications is a shift to a prothrombotic state, with 20% of hospitalized patients reporting thromboembolic events and an increased risk for blood clot-related issues, such as heart attack and stroke, which can last up to a year after infection[1, 2, 6, 7]. The frequency of these complications during and after SARS-CoV-2 infection is significantly higher than after infection with other respiratory viruses, suggesting this pathology is induced by effectors unique to SARS-CoV-2[8].

Indicators of endothelial cell (EC) activation and dysfunction, such as oxidative stress, hyperpermeability, endothelial-to-mesenchymal transition (EndoMT), hypercoagulability, and thrombosis have all been observed in SARS-CoV-2 infected patients [5]. However, *in vivo* direct infection of ECs remains controversial[9, 10]. Infection has, however, been detected in vascular smooth muscle cells and pericytes[11, 12]. Clot initiation begins with endothelial cells through both extrinsic and intrinsic pathways. The extrinsic pathway is initiated through tissue factor expression in perivascular cells, including smooth muscle cells. In addition, recently published data demonstrate that vascular smooth muscle cells are crucial mediators of endothelial cell function [13, 14]. Here, the extensive crosstalk between vascular endothelial cells and adjacent SMCs prompted us to examine if infection of SMCs cells could be the trigger for the endothelial cell dysfunction and thromboembolic events associated with infection.

Human pluripotent stem cells (hPSCs) can provide an unlimited, defined, and reproducible source of functional human cells for modeling diseases *in vitro*. In this report, we built off previously published approaches[15, 16] to generate a new protocol to produce uniform populations of ECs and perivascular cells, including SMCs and pericytes (PCs). We specifically developed this approach using a serum-free and common defined media for all three cell types to isolate the effects of culture conditions away from the cellular responses to SARS-CoV-2. Using these cells, we modeled SARS-CoV-2 vascular infection under defined conditions and investigated the cell-type specific response of vascular cells to SARS-CoV-2 exposure. Our results show a preferential tropism for perivascular cells over ECs and that SMCs are likely potent sites of SARS-CoV-2 infection. In addition, exposure to SARS-CoV-2 transforms SMCs into activators of coagulation signaling in ECs which may, in turn, contribute to the devastating vascular complications observed with SARS-CoV-2 infection in human patients. Finally, our system provides a physiologically relevant platform for further studies on drug development and modeling vascular pathogenesis in a defined system.

Results

A fully defined, efficient, and serum-free protocol allows for differentiation, culture, and maintenance of ECs, PCs, and SMCs from hPSCs with a single common medium.

We established a step-wise protocol to generate and maintain both perivascular cells (PC and SMC) and ECs in high purity (>97%) using a defined media **(Fig. 1A-B)**. Similar to previously published approaches[15, 16], the approach to generate ECs begins with mesendoderm specification using CHIR99021-mediated WNT activation and bone morphogenetic protein 4 (BMP4), followed by endothelial specification using vascular endothelial growth factor (VEGF), forskolin, and inhibition of platelet-derived growth factor receptor (PDGFR) and transforming growth factor beta (TGFβ) signaling, and a last stage of purification with n-cadherin inhibition, and continued PDGFR and TGFβ inhibition, and maturation with sphingosine-1-phosphate (S1P) **(Fig. 1A, Supplemental Fig. 1A-B)**.

Alternatively, after mesendoderm and early vascular specification, PDGF addition with TGFβ inhibition or TGFβ addition with PDGFR inhibition allowed for the derivation of PCs and SMCs **(Fig. 1B)**, respectively, in the same culture medium comprised of vascular base media comprising of Gibco Vascular SFM™, heparin, B27, epithelial growth factor (EGF), basic fibroblast growth factor (bFGF), and L-ascorbic acid-2-phosphate. All cells could be maintained and freeze-thaw recovered in the same common medium with the addition of PDGF for PCs and VEGF for ECs.

For ECs, these steps resulted in >85% purity as measured by VE-Cadherin (VE-Cad/CD144) and PECAM1 (CD31) **(Fig. 1B and Supplemental Fig. 1C)**, which could be enriched further via FACS and maintained after recovery to greater than >98% purity **(Fig. 1B Supplemental Fig. 1C)**. In addition, the ECs expressed canonical endothelial-related genes **(Fig. 1B)** and were capable of forming 3D networks in microfluidic devices with Matrigel **(Supplemental Fig. 1D)**. SMCs and PCs are two perivascular cell types that have been previously classified as contractile and non-contractile perivascular cells and characterized as both being PDGR positive. The delineation between the two is made through high or low levels of expression of smooth muscle actin (SMA)[15, 17, 18]. Similarly, we captured these differences via gene expression in the two perivascular cell populations derived here with higher levels of contractile-related genes SM2AA, CNN1, TAGLN, and aSMA in SMCs and higher levels of PDGFRa/b and vascular adhesion molecules VCAM1 and ICAM1 **(Fig. 1B)**. Additionally, immunohistochemistry of the two cells showed lower levels of expression in SMA and higher levels of NG2 and PDGFR in PCs relative to SMCs **(Fig. 1B)**. Importantly, relative to previously published protocols[15, 16], both of these perivascular cells were derivable in high purity (>97%), as shown in **Fig. 1B** and **Supplemental Figs. 1E-F** represented by the expression of PDGRb and SMA for SMCs and NG2 expression for PCs. PCs additionally expressed intermediate levels of both PDGFRa and PDGFRb relative to fibroblasts and the starting hPSC population **Fig. 1B** and **Supplemental Figs. 1E-F**, and both cell types could be subsequently cultured in the common and serum-free medium. Importantly, this parallel derivation in the same base, serum free, and defined media specifically allowed for the comparative infection studies in one common infection

medium (SMC medium) without the confounding variables of different or undefined media formulations.

SARS-Cov-2 demonstrates preferential tropism for human perivascular cells.

To assess the potential of hPSC-derived SMCs, PCs, and ECs to be infected by SARS-CoV-2, we exposed the differentiated cells to live SARS-CoV-2 and collected media at 24 and 48 hours post-exposure. We quantified the amount of infectious virus via plaque assays and found increased infectious virus in the media from SMCs and PCs, indicating that both cell types were productively infected with SARS-COV-2 **(Fig. 1C)**. Notably, SMCs showed the highest amount of released virus over a 48-hour infection **(Fig. 1C)**. Conversely, exposure of ECs to SARS-CoV-2 resulted in no subsequent release of infectious virus in the media, suggesting that these cells are not productively infected with SARS-CoV-2 **(Fig. 1C)**. Double-stranded RNA (dsRNA) is produced during SARS-CoV-2 genome replication[19]. In agreement with the plaque assay data, we detected dsRNA in a subset of hPSC-derived PCs and SMCs, indicating active viral replication, but not in ECs **(Supplemental Fig. 1G).** Collectively, these data support published reports that primary endothelial cells are likely not primary targets of SARS-CoV-2 infection[9]. The striking difference in the susceptibility of SMCs and ECs to SARS-CoV-2 infection prompted us to compare the transcriptional response of these two cell types to SARS-CoV-2 exposure.

SARS-CoV-2 exposure drives divergent transcriptomic responses in human SMCs and ECs

To identify the transcriptional changes induced by SARS-CoV-2 infection, we performed bulk RNA sequencing on hPSC-derived ECs and SMCs exposed to SARS-CoV-2. Although our results showed that ECs are not productively infected with SARS-CoV-2, previous reports have demonstrated that exposure to SARS-CoV-2 proteins is sufficient to impair EC function[20]. In the model developed here, human ECs and SMCs exposed to SARS-CoV-2 showed significant changes in gene expression **(Fig. 2A-B).** Notably, however, in ECs the changes in gene expression appeared

only to reflect their response to SARS-CoV-2 virions, as there were negligible differentially expressed genes in EC exposed to live vs. heat-inactivated (HI) SARS-CoV-2 **(Fig. 2C)**. Heat inactivation has previously been shown to disrupt the SARS-CoV-2 virion resulting in a non-infectious, but intact virion, indicating that subsequent findings in ECs here reflect EC response to surface viral proteins[21]. In contrast to ECs, SMCs responded more significantly to SARS-CoV-2 infection **(Fig. 2B)** with respect to differentially expressed genes, with, as expected, SARs-CoV-2 RNA being enriched in the infectable SMC "upregulated" genes **(Fig. 2B)**. In addition, there were distinct differentially expressed genes in live versus HI SARS-CoV-2 conditions, **(Fig. 2D)**, indicating that SMCs both respond to the viral proteins directly, as well as have distinct changes in gene expression upon actual infection.

Gene set enrichment analysis (GSEA)[22] for cells exposed to either live or heat-inactivated SARS-CoV-2 showed divergent pathway responses in ECs and SMCs. In ECs treated with either live or HI SARS-CoV-2, we observed upregulation of genes associated with the reactive oxygen species pathway **(Fig. 3A, C)**. SMCs exposed to both live and HI SARS-CoV-2 showed a robust enrichment in the interferon α and interferon γ innate immune response pathways **(Fig. 3B, D)**. Notably, the induction of inflammatory pathways was significantly higher in SMCs exposed to live virus as opposed to heat-inactivated virus **(Supplemental Fig. 2)**. In both cell populations, we observed gene set upregulation of generic metabolic (oxidative phosphorylation, adipogenesis, fatty acid metabolism, etc.,), cell cycle (G2M checkpoints, mitotic spindle, Myc targets, etc.,), as well as, expected, cell death (DNA repair and apoptosis) related genes **(Fig. 3A-D)**.

To confirm the finding that EC exposure to SARS-CoV-2 increased the generation and response to reactive oxygen species (ROS), ECs were then incubated with CellROX Green Reagent to detect generation of ROS by immunofluorescence. A significant increase in ROS signal was detected in ECs exposed to both live and heat-inactivated SARS-CoV-2 for 48 hours **(Fig. 3E-F)**. Collectively these data both support our initial finding that SMCs are the susceptible vascular cell to SARS-CoV-2 infection as well as further show that infection and the presence of virions amplifies the divergent

responses in ECs and SMCs, specifically of reactive oxygen species and induction of innate immune signaling respectively. Lastly, while these data indicate that exposure to the viral particles were sufficient to induce endothelial dysfunction in the absence of any observed infection, treatment with free viral spike and nucleocapside proteins alone were not able to recapitulate this effect **(Supplemental Fig. 3)**.

Paracrine signaling from SARS-CoV-2 infected SMCs induces inflammatory signaling in ECs

As shown in our data above, exposing hPSC-derived ECs directly to SARS-CoV-2 virions did not induce significant innate immune signaling **(Fig. 2A,C and 3A,C)**. However, elevated inflammatory signaling is a key component of endothelial cell activation observed during SARS-CoV-2 infection[5]. We have demonstrated here that SMCs are a target for SARS-CoV-2 infection, and the crosstalk between SMCs and ECs has been previously shown to contribute to the pathology of vascular disease[13]. We hypothesized that ECs could be impacted by paracrine signaling from nearby infected SMCs. To test this hypothesis, we exposed ECs to media collected from infected SMCs (CoV-2 SMC CM) **(Fig. 4A)**. In addition, we collected media from SMCs exposed to HI SARS-CoV-2 (HI SMC CM) to identify any changes in SMC paracrine function in response to viral particles alone **(Fig. 4A)**. Exposure of ECs to either CoV-2 SMC CM or HI SMC CM resulted in significant changes in gene expression when compared to ECs exposed to media conditioned from uninfected SMCs **(Fig. 4B-C, Supplemental Fig. 4).**

We again performed GSEA and observed that both treatment conditions demonstrated induction of pathways that could potentially contribute to vascular dysfunction via the effects on ECs by infected neighboring perivascular cells such as SMCs. As before, we observed upregulation of genes associated with reactive oxygen species **(Fig. 4D-E)**; however, treatment with live or HI CoV-2 SMC CM increased the normalized enrichment scores for this pathway. Unlike the direct infection effects described in **Fig. 2A,C and 3A,C,** this paracrine infection mimicking model now induced inflammatory signaling pathways in ECs, including IFN-α and IFN-γ response pathways, and TNFα signaling via

NF-κB **(Fig. 4D-E, Supplemental Fig. 5A)**. Notably, the induction of many genes in the interferon response pathways was significantly higher in EC exposed to CoV-2 SMC CM compared to EC exposed to HI SMC CM **(Supplemental Fig. 5B)**. Lastly, both transfer conditions resulted in further upregulation of the previously observed metabolic pathways as well as an increase in TGFβ-signaling known to regulate EndoMT[23, 24] and apoptosis **(Fig. 4D-E)**. Taken together, these data indicate that, while no substantial responses outside of increased reactive oxygen species-related gene signaling were detected after direct exposure, ECs' can be further impacted by the infection of nearby perivascular cells such as SMCs and subsequent exposure to resulting changes in the local paracrine environment. These further impacted gene response pathways include those a potential connection to vascular dysfunction (innate immune signaling, metabolic disruption, TGFβ-signaling, and cell death).

Paracrine signaling from SARS-CoV-2 infected SMCs initiates coagulation pathways in ECs

In addition to the enriched pathways described, we also observed that exposing ECs to media from infected or HI-exposed SMCs significantly upregulated the expression of multiple genes involved in coagulation **(Fig. 4D-E and 5A-B).** Included in the coagulation gene set[25] was SERPINE1, a known inhibitor of plasminogen (PA-1) and a blood biomarker of which elevated plasma levels have been observed in patients with severe SARS-CoV-2 infection[26] **(Fig. 5A-B)**. To determine if the exposure of ECs to media from infected SMCs also increased protein secretion, we measured SERPINE1 protein levels in the media from ECs exposed to CoV2 SMC CM for 48 hours. ECs exposed to CoV-2 SMC CM released significantly more SERPINE1 than ECs exposed to control SMC media **(Fig. 5C)**. Similar to SERPINE1, increased plasma levels of von Willebrand Factor (vWF), a blood glycoprotein involved in clotting released from activated ECs and a common biomarker for coagulopathies[27], has been observed in patients with severe SARS-CoV-2 infection[26, 28]. ECs exposed to CoV-2 SMC CM also released significantly more vWF into the media than ECs exposed to control SMC media **(Fig. 5D)**. We propose that these data suggest the observed coagulopathy-related vascular dysfunction

observed in human patients infected with SARS-CoV-2 may be related, in part, to the paracrine effects induced by neighboring infected SMCs and the resulting increased prothrombotic signaling from ECs.

Infected SMCs release factors that increase brain microvascular endothelial cell permeability

Intracerebral hemorrhage (ICH) can be a rare but devastating consequence of SARS-CoV-2 infection [29]. Disruption of the blood-brain barrier is a hallmark of ICH-induced brain injury[30]. hPSC-derived brain microvascular endothelial cells (hBMECs) recapitulate much of the unique physiology of the brain microvascular endothelial cells in the blood-brain barrier [31, 32]. As we observed clear dysfunction in the more peripheral-like ECs after exposure to infected perivascular cells, we applied the paracrine-infection model developed here to further understand the role of SARS-CoV-2 infection on the specialized subsets of ECs in the brain using hBMECs. Similar to the peripheral ECs, hBMECs exposed to live virus for 24 or 72 hours and stained with an antibody against dsRNA showed little to no infection, indicated by rare dsRNA-positive cells at the 72 hour time point **(Supplement Fig. 6A)**. These data are in agreement with a previous report that showed a low level of infection by 72 hours in primary BMECs[33]. The induction of inflammatory signaling has the potential to disrupt BMEC barrier function through the downregulation of tight junction proteins[34]. As our previous results **(Fig. 4D and Supplemental Fig. 5)** indicated that infected SMCs release factors that promote inflammatory signaling in ECs, we hypothesized that similar signaling would result in decreased barrier integrity in hBMECs. Transendothelial electrical resistance (TEER) provides a quantitative measurement of junctional tightness[35]. TEER was measured in hBMECs that were plated in transwell plates and exposed to either CoV-2 SMC CM or HI SMC CM over the course of 72 hours. We observed a significant reduction in TEER values over time in hBMECs exposed to CoV-2 SMC CM **(Fig. 5E)**, whereas no reduction was observed in hBMECs exposed to HI CoV-2 CM **(Supplemental Fig. 6B)**.

hPSC-derived SMCs increase tissue factor expression and activity in response to SARS-CoV-2 infection and constitute a platform for identifying targeted antiviral therapies

Tissue factor (TF) is a key initiator of the extrinsic blood coagulation pathway expressed in vascular smooth muscle cells following injury[36], and in the lungs of patients with severe SARS-CoV-2 infection[37, 38]. To determine if SARS-CoV-2 infection of SMCs resulted in increased TF expression, SMCs were exposed to either live SARS-CoV-2 or heat-inactivated SARS-CoV-2 and stained with an antibody against TF. Exposure to live SARS-CoV-2 resulted in an increase in TF staining in SMCs **(Fig. 6A-B)**, which appeared to correlate with dsRNA positive cells **(Supplemental Fig. 7A)**. Quantifying the average intensity of SMCs expressing TF, we observed this increase was specific to live SARS-CoV-2 infection **(Fig. 6C)**. To further determine whether the increased surface expression of TF indicated functional activation, we employed an enzyme-linked immunosorbent assay (ELISA) to quantitate TF activity from lysate of SMCs exposed to live or heat-inactivated SARS-CoV-2. Our data showed significantly higher TF activity in the lysate from SMCs infected with SARS-CoV-2 **(Fig. 6D).** Collectively, these data suggest that the upregulation of TF is a direct effect of infection and gives additional cellular mechanistic insight into how SARS-CoV-2 and the tropism shown here might cause the unique vascular dysfunction observed in COVID-19 patients.

Given that our data here suggest that infection of SMCs may be one of the major initiating factors in the development of the vascular pathology associated with infection, we sought to determine whether inhibiting known viral infection pathways in perivascular cells would blunt this, as a proof-of-principle of this model's use in drug development in infectious disease with vascular complications. The sphingolipid synthesis pathway has been shown to play a critical role in the replication of viruses and regulation of the innate immune response[39] and is involved in the development and maturation of blood vessels[40, 41]. Modulation of this pathway has been proposed as a potential therapeutic treatment for severe infection[42]. To determine if inhibition of sphingolipid signaling in SMCs could reduce SARS-CoV-2 infection, SMCs were treated with N,N-Dimethyl-D-erythro-sphingosine (DMS), which inhibits the phosphorylation of sphingosine to form sphingosine 1-phosphate. Treatment with

DMS resulted in a dose-dependent reduction of infectious virus production in SMCs, which could not be accounted for by the toxicity of the drug **(Supplemental Fig. 7B)**.

Discussion

The SARS-CoV-2 pandemic has impacted millions of people worldwide. The vascular complications that arise from severe infection continue to devastate patients long after the peak of infection. One year after infection, patients who were infected with SARS-CoV-2 are 63% more likely to have cardiovascular issues and have a 52% increased risk of stroke[7]. In this report, we present a model system to study the tropism and pathology associated with SARS-CoV-2 vascular infection. Our data demonstrate that within the vasculature, perivascular cells, including pericytes and smooth muscle cells, are major targets for SARS-CoV-2 infection. Also consistent with previous reports[9], our results here show no evidence of productive viral infection in human ECs. These data are particularly relevant in light of recent studies using patient biopsy samples which showed evidence of the spread of infection through the bloodstream during an early viremic phase[12]. This systemic spread likely results in virus throughout the body following infection of the respiratory tract[12].

While we did not observe any productive infection of ECs, the RNA seq data did show perturbation of EC gene expression by exposure to SARS-CoV-2 **(Fig. 2)**. To better understand the direct effects on vascular endothelium from SARS-CoV-2 exposure in the absence of infection, we exposed ECs to both live and HI SARS-CoV-2 particles. The absence of significant differences following live versus HI exposure in ECs suggests the direct impact on vascular endothelium could be due to interactions between ECs and the viral proteins present on the surface of the viral particle. This finding is in line with a previous study in hamsters using pseudotyped virus expressing SARS-CoV-2 spike protein[20]. Lastly, these effects were not observed with free recombinant nucleocapsid or spike protein, indicating viral particle presentation of these proteins may be required **(Supplemental Fig.3).**

In identifying the sites of vascular infection, we also observed that only a subset of SMCs and PCs were positive for dsRNA staining **(Supplemental Fig. 1 & Supplemental Fig. 7)**. This may be due to heterogeneity in receptor expression, or alternatively, the viral genomic replication which produces dsRNA may be quickly dampened by the host cell's innate immune responses[43]. *In vivo,* likely only small percentage of interactions between viral particles and cells result in productive infection due to both the production of defective viral particles [44] as well as interactions of infectious viral particles with cells that are not susceptible to SARS-CoV-2 infection. However, our results comparing the transcriptional response of SMCs and ECs exposed to live virus versus heat-inactivated virus allowed us to discriminate between transcriptional changes that are due to productive infection as well as changes that are induced via exposure to viral particles without downstream infection. Our results suggest that the overall SMC response may be sufficient to promote vascular dysfunction and prompted us to expand our model to mimic paracrine effects on ECs produced by neighboring infected and exposed SMCs.

Contrary to the limited dysfunction beyond endothelial ROS responses observed in our initial model of direct infection, the paracrine model showed significant dysregulation of vascular gene pathways in ECs. Specifically, we observed increased expression of genes in interferon response pathways, further reactive oxygen species, and significant cell death in ECs exposed to the SMC paracrine milieu. Moreover, the data showed that SMCs exposed to heat-inactivated SARS-CoV-2 alone, which cannot initiate infection, release factors that promote coagulation signaling in ECs, suggesting that exposure of SMCs to circulating viral particles may be sufficient for activation of coagulation pathways through an SMC dependent mechanism. Lastly, the conditioned medium model combined with another hPSC-derived cell type, hBEMCs, provided mechanistic insights into how neighboring SARS-CoV-2 infected perivascular cells can contribute to vascular dysfunction such as leakage and edema through decreasing barrier function.

The approach detailed here describes a highly efficient manner for deriving pure perivascular and endothelial cells from hPSCs in a defined and common media for use in infectious disease modeling. Using the defined and serum-free conditions for all cell types, this model could be used to study the tropism of SARS-CoV-2 on cells of the vasculature. The model and results described here add to the existing literature that perivascular cells, not the endothelium, are the target sites of infection. However, viral particles themselves can alter the state of ECs in the absence of infection. Additionally, the defined common medium format for all cell types allowed us to perform a set of conditioned media experiments without the complications of different media compositions and then model the outcomes of paracrine changes in the EC microenvironment from infection of neighboring perivascular cells. This approach ultimately provided a potential intrinsic and extrinsic mechanism for coagulopathies associated with SARS-CoV-2 and paradoxical vascular leakage and edema. In summary, our findings add to the knowledge of the relationship between the unique vascular complications associated with SARS-CoV-2 infection and COVID-19 patients, and provide a highly efficient derivation of a fully defined and serum-free hPSC vascular model.

Data availability

An accompanying data file is available with this submission, containing the raw values for all figures. RNA seq raw data is uploaded to Gene Expression Omnibus. Additional reasonable data requests will be made available from the corresponding authors.

Acknowledgments

We acknowledge funding from the Wellcome-LEAP HOPE initiative, NIH (T32 EB016652), the Wyss Institute, and the Whitehead Institute. We thank the Genome Technology Core and Keck Imaging Facility at Whitehead Institute for Biomedical Research. This work was supported by NIH grant U19AI131135-01, NIBIB grant T32 EB016652, and by a generous gift from Jim Stone. The following reagent was deposited by the Centers for Disease Control and Prevention and obtained through BEI Resources, NIAID, NIH: SARS-Related Coronavirus 2, Isolate USA-WA1/2020, NR-52281. This work

was performed in part in the Ragon Institute BSL3 core, which is supported by the NIH-funded Harvard University Center for AIDS Research (P30 AI060354).

Conflicts of Interest

R.J. is an advisor/co-founder of Fate Therapeutics, Fulcrum Therapeutics, Omega Therapeutics, and Dewpoint Therapeutics. D.J.M. has sponsored research from Novartis, consults, and/or has stock options/stock in J&J, Medicenna, Boston Scientific, Lyell, Attivare, IVIVA, Epoulosis, Limax Biosciences, and Revela.

Methods

hPSC lines and maintenance

H1 (WA01) embryonic stem cells were obtained from WiCell. hPSCs were maintained in feeder-free conditions in mTeSR Plus media (StemCell Technologies) on Matrigel (Corning) in 6-well tissue culture dishes. For passaging, hPSCs were detached as clumps using Versene Solution (Thermo Fisher Scientific) and replated at a ratio of 1:8-1:10.

Directed differentiation of hPSCs to endothelial cells

All media recipes are described in Table 2. H1 hPSCs were cultured in E8 media (Thermo Fisher Scientific) and dissociated using Accutase (Thermo Fisher Scientific) into a single cell suspension and plated at 15,000 cells/cm^2 in E8 media with Y-27632 (10µM) and onto Matrigel-coated tissue culture plates. Y-27632 was removed after 24 hours, and cells were cultured in E8 media until they reached approximately 70% confluency, at which point the media was replaced with MelM media; this is considered day 0. On day 2, the media was replaced with EC1 media. On day 5, the media was replaced with EC2 media for 24 hours, and then cells were passaged 1:1 onto fibronectin (FC01010MG, Fisher Scientific) coated tissue culture plates in EC3 media. Plates were coated with fibronectin at 10ug/ml for 30 minutes at 37°C prior to the addition of cells. After 48 hours, media was replaced with EC4 media for 5 days and then sorted for VE-Cadherin and PECAM1 double-positive cells using FACS. Sorted cells were plated back onto fibronectin and cultured for an additional 5 days in EC4 before cryopreservation or extended expansion in EC5 medium.

Directed differentiation of hPSCs to pericytes

All media recipes are described in Table 2. H1 hPSCs were cultured in E8 media (Thermo Fisher Scientific) and dissociated using Accutase (Thermo Fisher Scientific) into a single cell suspension and plated at 15,000 cells/cm^2 in E8 media with Y-27632 (10µM). Y-27632 was removed after 24 hours and cells cultured in E8 media until they reach approximately 70% confluency at which point

the media was replaced with MelM media , this is considered day 0. On day 2 the media was replaced with PC/SMC1 media. On day 5 the media was replaced with PC/SMC2 media for 24 hours and then cells were passaged 1:3 on to fibronectin (FC01010MG, Fisher Scientific) coated tissue culture plates in PC3 media. Plates were coated with fibronectin at 10ug/ml for 30 minutes at 37°C prior to the addition of cells. After 48 hours media was replaced with PC4 media. After 48 hours media was replaced with fresh PC4 and cells kept in culture for 7 days prior to freezing.

Directed differentiation of hPSCs to smooth muscle cells

All media recipes are described in Table 2. H1 hPSCs were cultured in E8 media (Thermo Fisher Scientific) and dissociated using Accutase (Thermo Fisher Scientific) into a single cell suspension and plated at 15,000 cells/cm^2 in E8 media with Y-27632 (10µM). Y-27632 was removed after 24 hours and cells cultured in E8 media until they reach approximately 70% confluency at which point the media was replaced with MelM media , this is considered day 0. On day 2 the media was replaced with PC/SMC1 media. On day 5 the media was replaced with PC/SMC2 media for 24 hours and then cells were passaged 1:3 on to fibronectin (FC01010MG, Fisher Scientific) coated tissue culture plates in SMC3 media. Plates were coated with fibronectin at 10ug/ml for 30 minutes at 37°C prior to the addition of cells. After 48 hours media was replaced with SMC4 media. After 48 hours media was replaced with SMC5 and cells kept in culture for 7 days prior to freezing.

Directed differentiation of hPSCs to brain microvascular endothelial cells

The differentiation of H1 hPSCs to brain microvascular endothelial cells was based on a previously published protocols[31, 45, 46]. Briefly, hPSCs were dissociated using Accutase (Thermo Fisher Scientific) into a single cell suspension and plated at 15,000 cells/cm^2 in StemFlex media with Y-27632 (10µM). Y-27632 was removed after 24 hours and at 48 hours post-plating the media was replaced with Unconditioned Media (UM) (100ml Knock-out Serum Replacement (Thermo Fisher Scientific), 5ml non-essential ammino acids (Thermo Fisher Scientific), 2.5ml GlutaMax (Thermo

Fisher Scientific), 5ml Pen/Strep (Thermo Fisher Scientific), 3.5µl β-mercapto-ethanol (Sigma), and 392.5ml DMEM/F12(1:1)), this was considered day zero. The media was replaced daily with fresh UM. On day six the media was changed to hESFM (Thermo Fisher Scientific) supplemented with 20 ng/mL bFGF (Peprotech), 10 µM retinoic acid (RA) (Sigma), and 1:50 B27 (Thermo Fisher Scientific). The media was not changed for 48 hours. On day eight, cells were washed once with DPBS and incubated with Accutase for 30 minutes at 37°C. Cells were collected via centrifugation and plated onto either standard tissue culture plates or transwell plates (Corning #3460). Both plates and transwells were coated with 400 µg/mL collagen IV (Sigma Aldrich) and 100 µg/mL fibronectin (Fisher Scientific) overnight with collagen and fibronectin and washed 1X with PBS prior to the addition of cells. For tissue culture plates, cells were plated at a density of 250,000 cells/cm^2, whereas for transwell plates, cells were plated at a density of 1.1 x 10^6 cells/cm^2 on the transwell membrane. bFGF and RA were removed from the medium 24 hours after plating.

SARS-CoV-2 propagation, titration, and inactivation

SARS-CoV-2 (isolate USA_WA1/2020) was obtained from BEI Resources. The virus was propagated in Vero E6 cells (ATCC CRL-1586) cultured in Dulbecco's modified Eagle's medium (DMEM) supplemented with 2% fetal calf serum (FCS), penicillin (50 U/mL), and streptomycin (50 mg/mL). SARS-CoV-2 titer was determined in Vero E6 cells by plaque assay. All work with SARS-CoV-2 was performed in the biosafety level 3 (BSL3) at the Ragon Institute (Cambridge, MA) following approved SOPs. To generate heat-inactivated SARS-CoV-2 a 1ml aliquot of SARS-CoV-2 was heated to 85°C for 15 minutes.

RNA Isolation, cDNA Preparation, and qRT-PCR

Total cellular RNA was extracted using the RNeasy Plus Mini kit (QIAGEN) following the manufacturer's protocol. cDNA synthesis was performed using qScript cDNA Supermix according to the manufacturer's instructions, using 1000ng RNA as input (qScript cDNA SuperMix, QuantaBio -

95048-500). qPCR was performed on a Thermo Fisher Scientific QuantStudio 6 machine using Fast SYBR™ Green Master Mix (Thermo Fisher Scientific 4385618). Expression data is presented after calculating the relative expression compared with the housekeeping gene RPLP0, using the equation Relative Quantification (RQ) = 100/(2ˆ(Target Gene Ct – RPLP0 Ct). When data is reported relative to a sample condition, the condition of reference was set as 1, and the data of the other conditions are reported as a ratio (condition/condition of reference). Data is reported from replicate differentiations.

Bulk RNA-sequencing of infected and exposed vascular cells

RNA was extracted using the RNeasy Plus Mini kit (QIAGEN) following the manufacturer's protocol. For bulk RNA sequencing of total RNA, libraries were prepared using the Swift RNA library prep kit (Swift Biosciences). Samples were sequenced on a NovaSeq 6000 sequencer.

Analysis of gene expression

Paired-end reads (51x 51 bp) were mapped to a reference genome using the STAR aligner (v. 2.7.1a)[47]. The reference genome was a composite of the human genome (GRCh38) and that of the SARS-CoV-2 coronavirus (GenBank MN988713.1). Counts for human protein coding genes and lncRNAs (ENSEMBL release 93 annotations), together with the viral genes, were tabulated using featureCounts[48]. Differential expression of mRNAs was assessed for pairwise contrasts between conditions using estimated fold-changes and the Wald statistic in DESeq2 (v. 1.36.0)[49]. Per-gene dispersions were estimated using all conditions, as within-condition variance was observed to be relatively uniform across conditions in exploratory analyses. Unless otherwise noted, empirical Bayes shrinkage was applied to fold-change estimates[50]. Gene-set enrichment analysis was carried out between pairs of conditions using GSEA (v. 4.1.0)[22] with counts that were normalized by DESeq2 and 1000 gene-set permutations were used to estimate p-values. Gene-sets that were tested for enrichment came from the Hallmark collection at the MSigDB[25].

Flow cytometry

For live surface marker staining, cells were trypsinized with TrypLE Express for ~5-7 or until cells detached. Cells were washed once with FACS staining buffer consisting of 2 mM EDTA and 0.5% BSA and centrifuged. Cells were then resuspended and incubated in FACS staining buffer and the respective fluorophore-conjugated antibodies for each cell type at the concentrations listed in Table 1. For SMC staining that included intracellular SMA, cells were fixed with 1% PFA after the trypsinization and washing step listed above for 20 min at room temperature. The cells were then permeabilized in 90% methanol in PBS at -20C for at least 24 hr. After permeabilization, cells were washed in FACS buffer and resuspended in FACS buffer containing 0.1% Triton X-100 and the respective antibodies listed in Table 1. All antibodies were done for 20-30 min at 4C and were followed by a wash with FACS buffer. Stained cells were analyzed on a BD Fortessa UV/Blue/Green/Red 4-laser flow cytometer. Cells were isolated as a population and then selected for singlets before setting gates to determine positive populations. Undifferentiated hPSCs served as biological controls for all stains.

Immunofluorescence microscopy

Cells were fixed with 4% paraformaldehyde for 15 minutes at room temperature. Fixed cells were permeabilized for 15 minutes using 0.1% TX-100. Cells were then blocked with 3% BSA in PBS for 1 hour at room temperature. Cells were incubated with primary antibodies (see Table 1) diluted in antibody buffer (0.01%TX-100 and 1%BSA in PBS) overnight at 4°C. Cells were washed with 0.05% Tween in PBS and incubated for 1 hour at room temperature with secondary antibodies (see Table 1) diluted in antibody buffer. FITC-Phalloidin was added at 1:2000 and DAPI at 1:5000 with secondary antibodies.

Imaging of reactive oxygen species production

Endothelial cells were exposed to SARS-CoV-2 for 48 hours. At 48 hours post-infection the media was removed and replaced with FluoroBrite media (A1896701, Thermo Fisher Scientific)

supplemented with 1:50 B27 and CellRox Green Reagent (C10444, Thermo Fisher Scientific) at a final concentration of 5μM. Cells were incubated at 37°C for 30 minutes then washed 3 times with PBS and imaged immediately after washing. Cells were kept in FluoroBrite with B27 throughout imaging.

SERPINE1 (PAI-1) and von Willebrand factor (vWF) release measurements

Endothelial cells (ECs) were exposed to media from infected or uninfected smooth muscle cells (SMCs) for 48 hours at which point the media was collected and analyzed for PAI-1 content using the Human Serpin E1/PAI-1 Quantikine ELISA Kit (DSE100, R&D Systems) according to the manufacturer's protocol. The same media was analyzed for vWF content using the Human Von Willebrand Factor ELISA Kit (ab223864, Abcam) according to the manufacturer's protocol.

Measurement of Tissue Factor Activity

At 48 hours post-infection SMCs were lysed and solubilized with 50 mM Tris-buffered saline (pH 8.0) containing 0.5% Triton X-100 or 0.1% Tween 20 at 4°C for 30 minutes. Samples were then centrifuged at 14000 rpm for 10 minutes, and the supernatant was collected for analysis. Tissue factor (TF) activity was measured using a human tissue factor activity assay kit (ab108906, Abcam) according to the manufacturer's protocol.

Measurement of transendothelial electrical resistance

BMECs were plated onto three transwell filters (Corning #3460) using the procedure described in "Directed Differentiation of hPSCs to brain microvascular endothelial cells." 48 hours after plating the media was removed from the apical side of the transwell and replaced with SMC-conditioned media. At each time point, the TEER was measured in three separate locations. All data are represented as mean ± standard deviation for these collective measurements. All results were confirmed in a minimum of two additional biological replicates (specific numbers of biological replicates are noted in

the main text). Following the medium change on day 0 of subculture to remove bFGF and RA, no further medium changes were performed for the duration of the experiments.

Figures:

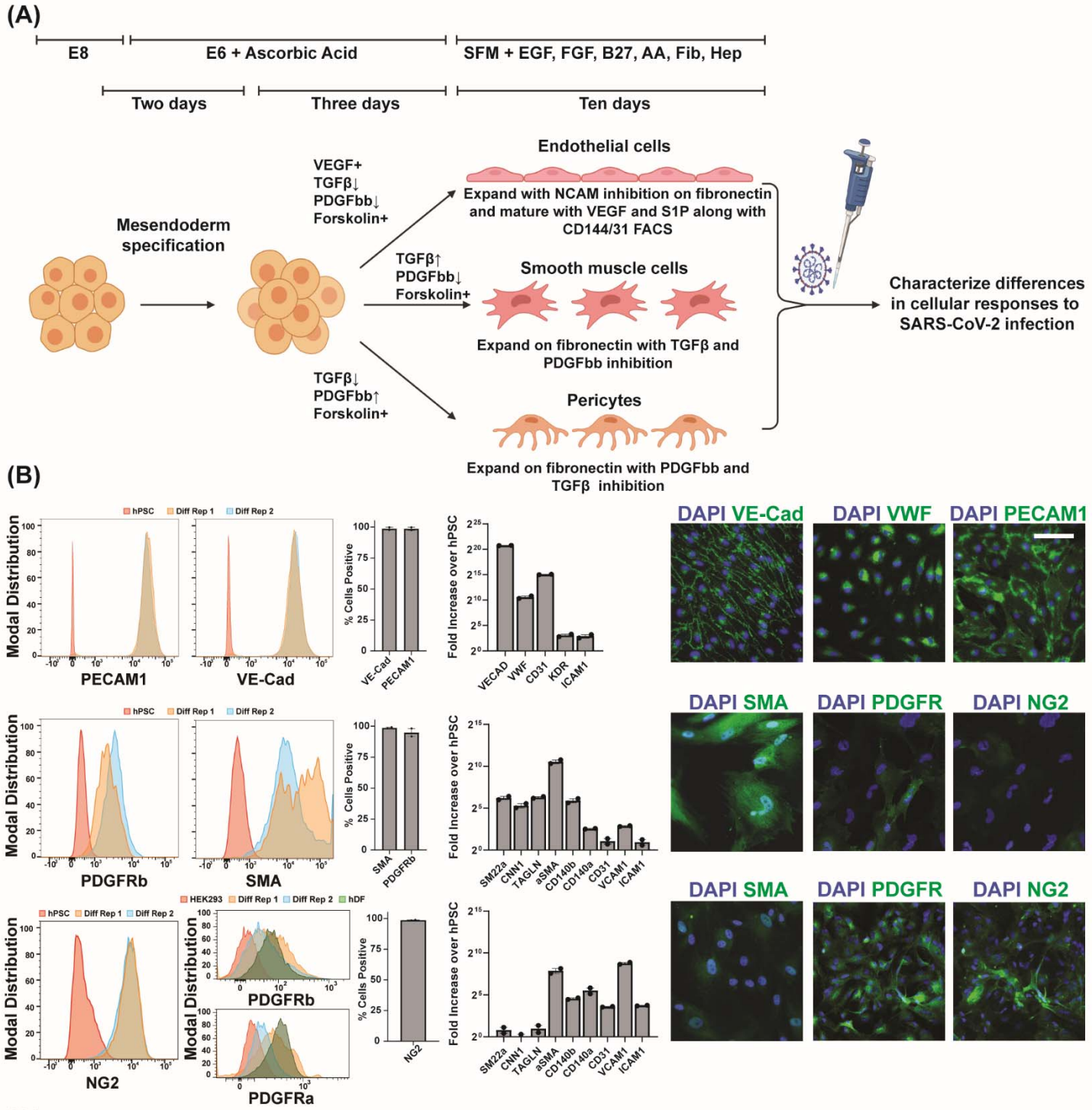
(A)
E8
E6 + Ascorbic Acid
SFM + EGF, FGF, B27, AA, Fib, Hep
Two days
Three days
Ten days
Mesendoderm specification
VEGF+
TGFβ↓
PDGFbb↓
Forskolin+
TGFβ↑
PDGFbb↓
Forskolin+
TGFβ↓
PDGFbb↑
Forskolin+
Endothelial cells
Expand with NCAM inhibition on fibronectin and mature with VEGF and S1P along with CD144/31 FACS
Smooth muscle cells
Expand on fibronectin with TGFβ and PDGFbb inhibition
Pericytes
Expand on fibronectin with PDGFbb and TGFβ inhibition
Characterize differences in cellular responses to SARS-CoV-2 infection
(B)
hPSC
Diff Rep 1
Diff Rep 2
HEK293
hDF
Modal Distribution
PECAM1
VE-Cad
PDGFRb
SMA
NG2
PDGFRa
% Cells Positive
Fold Increase over hPSC
VECAD
VWF
CD31
KDR
ICAM1
SM22a
CNN1
TAGLN
aSMA
CD140b
CD140a
VCAM1
DAPI VE-Cad
DAPI VWF
DAPI PECAM1
DAPI SMA
DAPI PDGFR
DAPI NG2
(C)
EC
PC
SMC
Plaque Forming Units/ml
Hours Post Infection
0
24
48

Figure 1: SARS-CoV-2 infection of hPSC derived vascular endothelial cells, smooth muscle cells, and pericytes (A) Schematic of directed differentiation of hPSCs to vascular endothelial cells (ECs), smooth muscle cells (SMCs) and pericytes (PCs). **(B)** hPSC derived ECs, SMCs, and PCs express cell-type specific markers as observed by flow cytometry, qRT-PCR, and immunofluorescence staining. Scale bar = 50 µm **(C)** SARS-CoV-2 infection of hPSC derived ECs, SMCs, and PCs. Amount of infectious virus released into the media at the indicated time post-infection was quantitated by plaque assay.

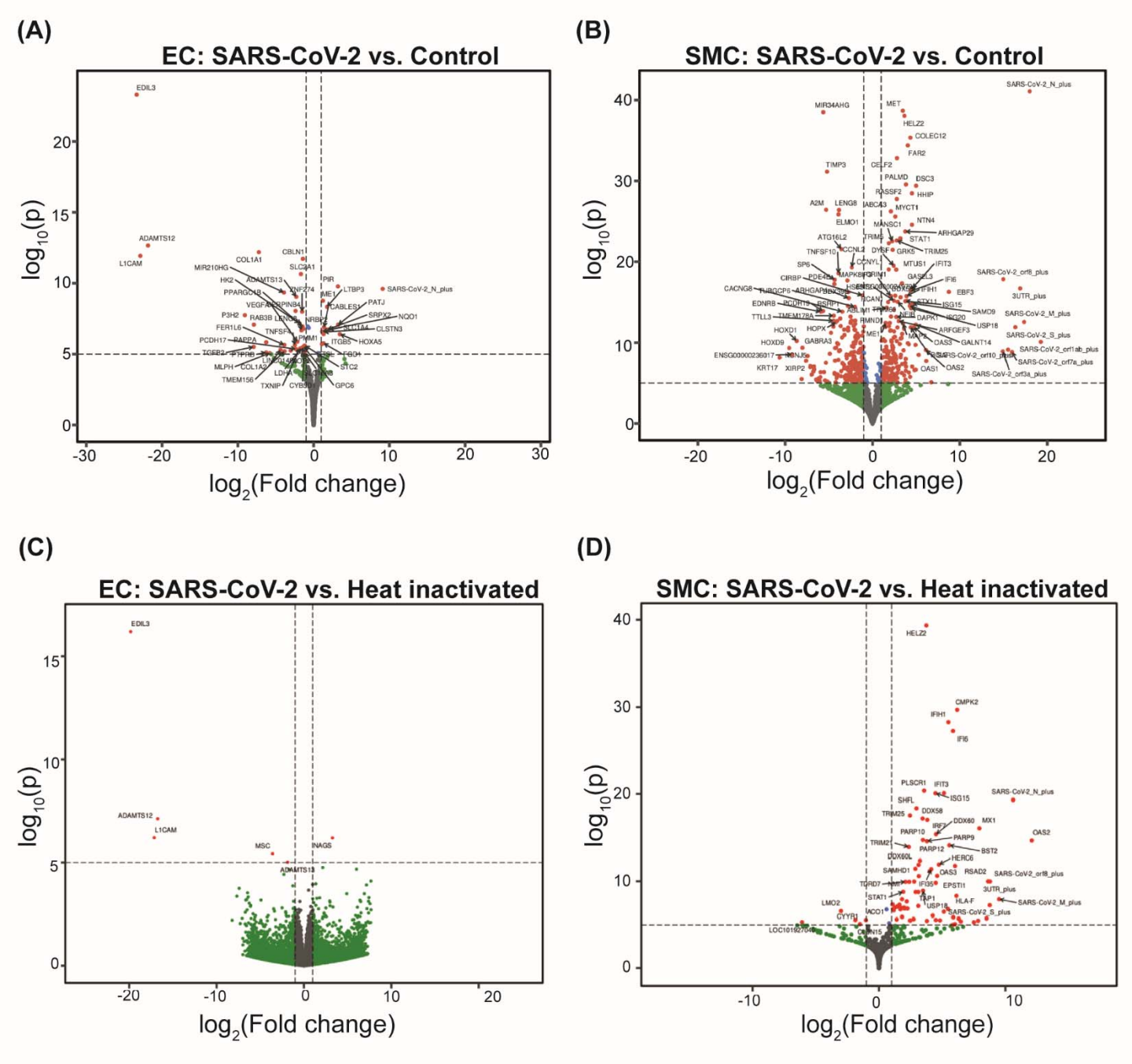

Figure 2: Gene expression changes in hPSC derived SMCs and ECs following exposure to SARS-CoV-2. Bulk RNA sequencing was performed on RNA isolated from hPSC-derived vascular ECs and SMCs 48 hours after virus exposure. Volcano plots showing differential gene expression in **(A)** ECs exposed to live SARS-CoV-2 compared to control uninfected ECs, **(B)** SMCs exposed to live SARS-CoV-2 compared to control uninfected SMCs, **(C)** ECs exposed to live SARS-CoV-2 compared to ECs exposed to heat-inactivated SARS-CoV-2 and **(D)** SMCs exposed to live SARS-CoV-2 compared to SMCs exposed to heat-inactivated SARS-CoV-2 (fold-change estimates shown without applying empirical Bayes shrinkage) .

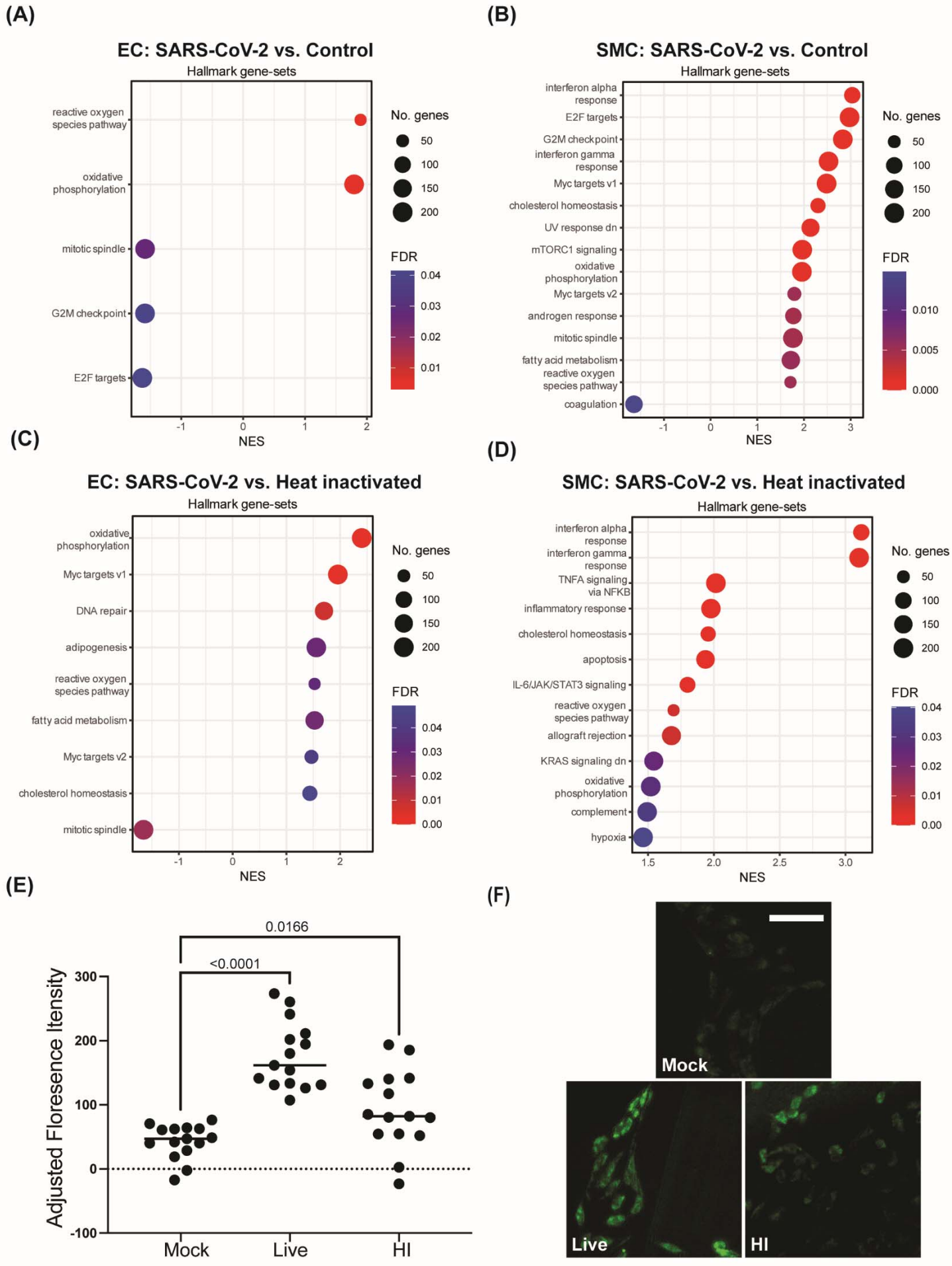
(A)
EC: SARS-CoV-2 vs. Control
Hallmark gene-sets
reactive oxygen species pathway
oxidative phosphorylation
mitotic spindle
G2M checkpoint
E2F targets
NES
No. genes
50
100
150
200
FDR
0.04
0.03
0.02
0.01
(B)
SMC: SARS-CoV-2 vs. Control
Hallmark gene-sets
interferon alpha response
E2F targets
G2M checkpoint
interferon gamma response
Myc targets v1
cholesterol homeostasis
UV response dn
mTORC1 signaling
oxidative phosphorylation
Myc targets v2
androgen response
mitotic spindle
fatty acid metabolism
reactive oxygen species pathway
coagulation
NES
No. genes
FDR
0.010
0.005
0.000
(C)
EC: SARS-CoV-2 vs. Heat inactivated
Hallmark gene-sets
oxidative phosphorylation
Myc targets v1
DNA repair
adipogenesis
reactive oxygen species pathway
fatty acid metabolism
Myc targets v2
cholesterol homeostasis
mitotic spindle
NES
No. genes
FDR
0.00
(D)
SMC: SARS-CoV-2 vs. Heat inactivated
Hallmark gene-sets
interferon alpha response
interferon gamma response
TNFA signaling via NFKB
inflammatory response
cholesterol homeostasis
apoptosis
IL-6/JAK/STAT3 signaling
reactive oxygen species pathway
allograft rejection
KRAS signaling dn
oxidative phosphorylation
complement
hypoxia
NES
No. genes
FDR
(E)
0.0166
<0.0001
Adjusted Floresence Itensity
300
200
100
0
-100
Mock
Live
HI
(F)
Mock
Live
HI

Figure 3: hPSC-derived ECs and SMCs display unique responses to SARS-CoV-2 exposure. Gene set enrichment analysis was performed on sequenced bulk RNA samples collected from SARS-CoV-2 exposed SMCs and ECs (Figure 2). Dot plots show gene-sets from the Hallmark collection[25] of the MSigDB that were enriched (FDR < 0.05) using gene-set enrichment analysis (GSEA)[22] to compare **(A)** ECs exposed to live SARS-CoV-2 versus control uninfected ECs, **(B)** SMCs exposed to live SARS-CoV-2 versus control uninfected SMCs, **(C)** ECs exposed to live SARS-CoV-2 versus ECs exposed to heat-inactivated SARS-CoV-2 and **(D)** SMCs exposed to live SARS-CoV-2 versus SMCs exposed to heat-inactivated SARS-CoV-2. (E) ECs were mock-infected or exposed to live or heat-inactivated SARS-CoV-2 at 48 hours post-infection. CellROX green reagent was added at a final concentration of 5 μM and incubated for 30 minutes at 37°C, and cells were analyzed by fluorescence microscopy. Green fluorescent signal showed the ROS-mediated oxidation of the reagent. The fluorescence intensity was measured for five cells from each of three fields of view per condition. **(F)** Representative image of CellRox staining at 48 hours post-infection.

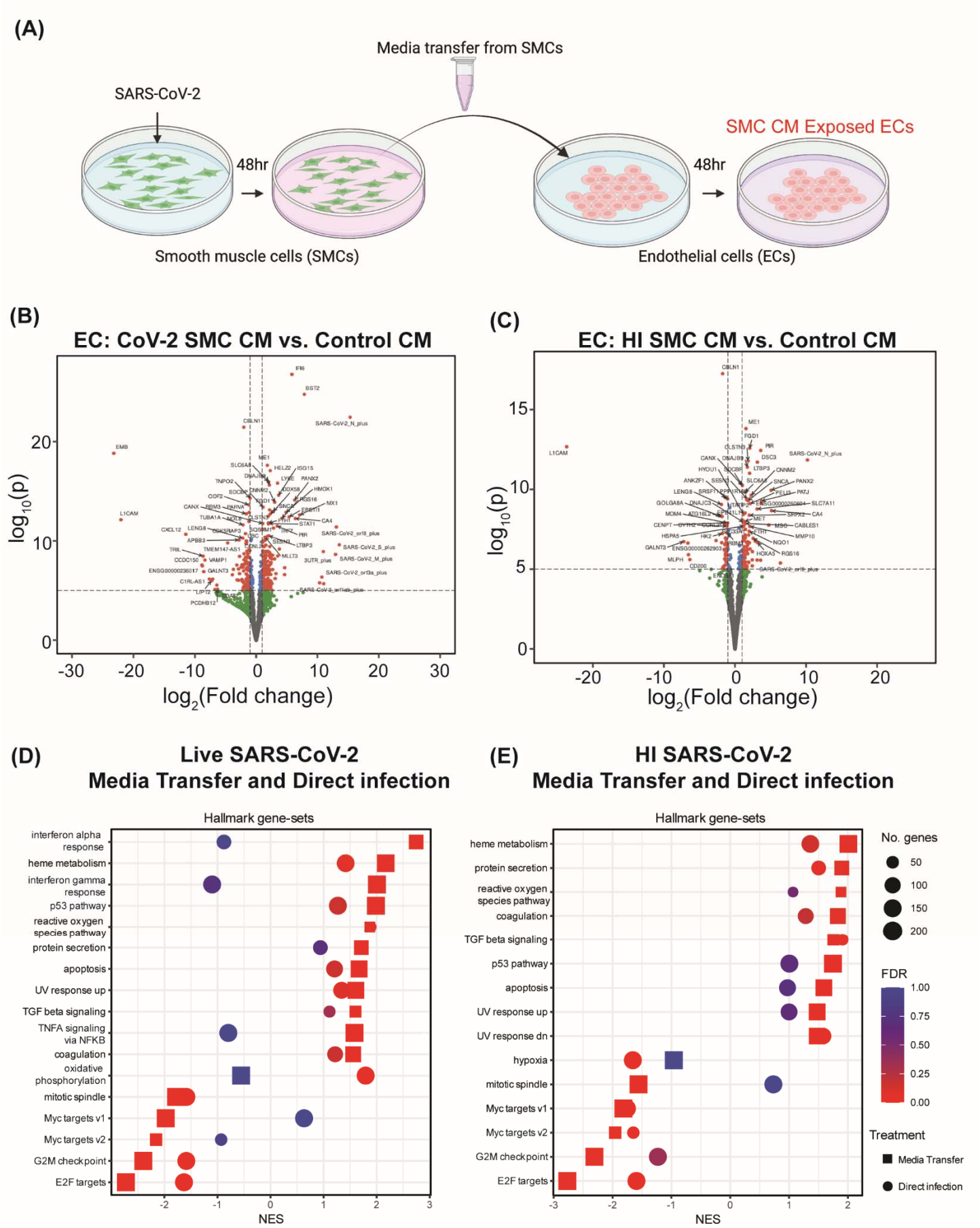

Figure 4: Paracrine signaling from SMCs exposed to SARS-CoV-2 alters EC gene expression

(A) Schematic of the experiment examining the effect of SMC-secreted factors on ECs. **(B-E)** Bulk RNA sequencing was performed on RNA isolated from ECs 48 hours after exposure to SMC conditioned media **(B)** Volcano plot of differentially expressed genes in ECs exposed to media from SARS-CoV-2 infected SMCs (*CoV-2 SMC CM*) compared to ECs exposed to media from uninfected SMCs *(Control CM)*. **(C)** Volcano plot of differentially expressed genes in ECs exposed to media from SMCs exposed to heat-inactivated SARS-CoV-2 *(HI SMC CM)* compared to ECs exposed to media from uninfected SMCs *(Control CM)*. **(D)** Dot plot summary of GSEA[22] comparing ECs exposed to media from SARS-CoV-2 infected SMCs with ECs exposed to media from uninfected SMCs (*Media Transfer*) plotted together with GSEA results for ECs exposed to live SARS-CoV-2 compared to control uninfected ECs (*Direct Infection*) **(E)** Dot plot summary of GSEA comparing ECs exposed to media from SMCs exposed to heat-inactivated SARS-CoV-2 with ECs exposed to media from uninfected SMCs (*Media Transfer*) plotted together with GSEA results for ECs exposed to heat-inactivated SARS-CoV-2 compared to control uninfected ECs (*Direct Infection*). In (**D**) and (**E**), the Hallmark collection[25] of gene-sets from the MSigDB was used and gene-sets were plotted only when FDR < 0.05 for enrichment in at least one of the between-condition comparisons.

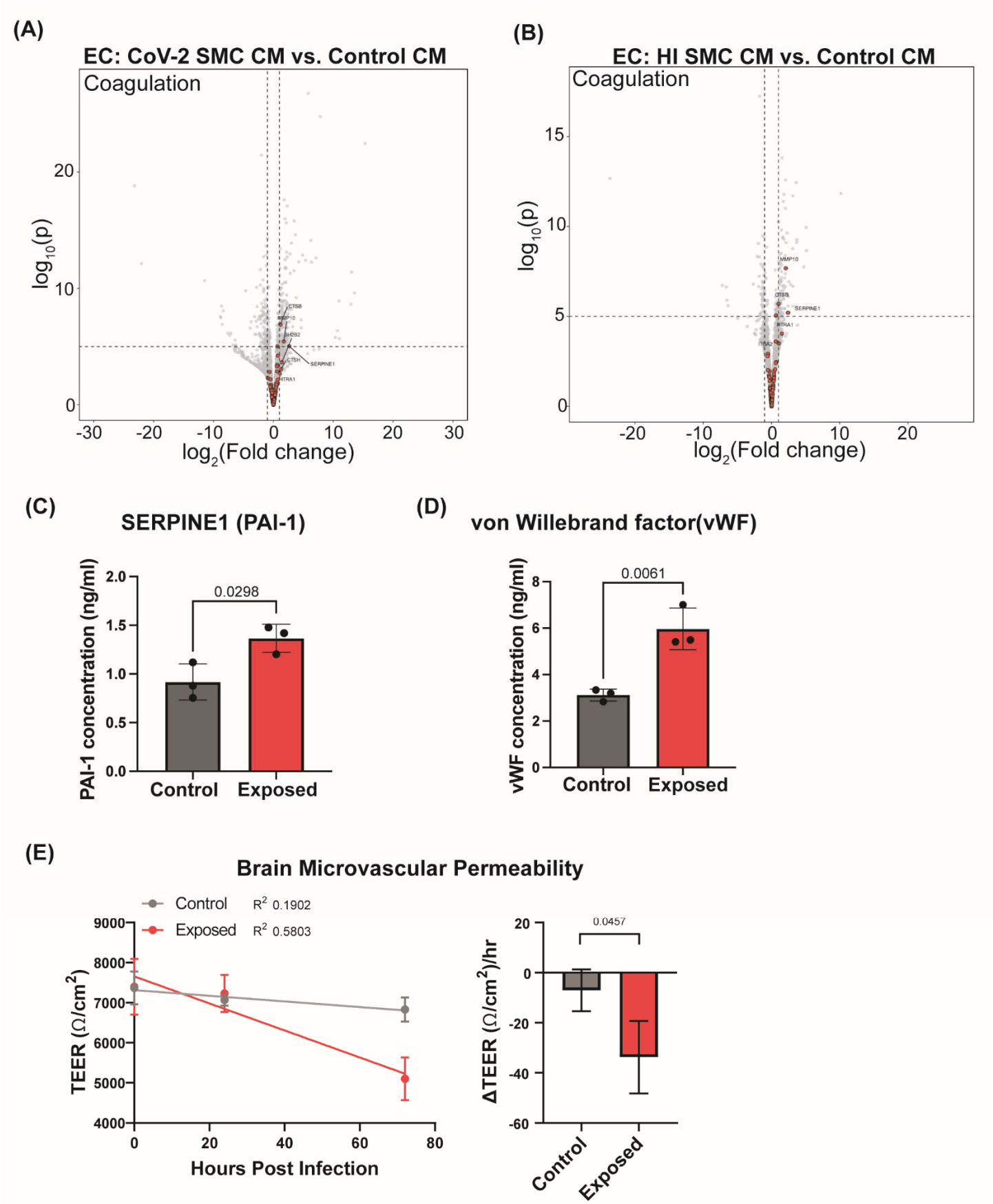

Figure 5: SARS-CoV-2 exposed SMCs release factors that promote clotting and reduce barrier function in ECs. (A, B) Bulk RNA sequencing was performed on RNA isolated from ECs 48 hours

after exposure to SMC-conditioned media (Figure 4) **(A)** Volcano plot for differential gene expression in ECs exposed to media from SARS-CoV-2 infected SMCs (*CoV-2 SMC CM*) compared to ECs exposed to media from uninfected SMCs *(Control CM)*. **(B)** Volcano plot for differential gene expression in ECs exposed to media from SMCs exposed to heat-inactivated SARS-CoV-2 *(HI SMC CM)* compared to ECs exposed to media from uninfected SMCs *(Control CM)*. In both (**A**) and (**B**), genes highlighted in red correspond to the "coagulation" gene-set from the Hallmark collection[25] of the MSigDB, with GSEA[22] "leading edge" genes labeled by name. **(C)** Quantitation of SERPINE1(PAI-1) in the media of ECs exposed to media from SARS-CoV-2 infected SMCs (*Exposed*) and ECs exposed to media from uninfected SMCs *(Control)*. **(D)** Quantitation of von Willibrand Factor (vWF) in the media of ECs exposed to media from SARS-CoV-2 infected SMCs (*Exposed*) and ECs exposed to media from uninfected SMCs *(Control)*. **(E)** Trans-endothelial cell electrical resistance (TEER) was measured at 0, 24, and 72 hours after exposure of hPSC-derived brain microvascular endothelial cells to media from SARS-CoV-2 infected SMCs (*Exposed*) or media from uninfected SMCs (*Control)*.

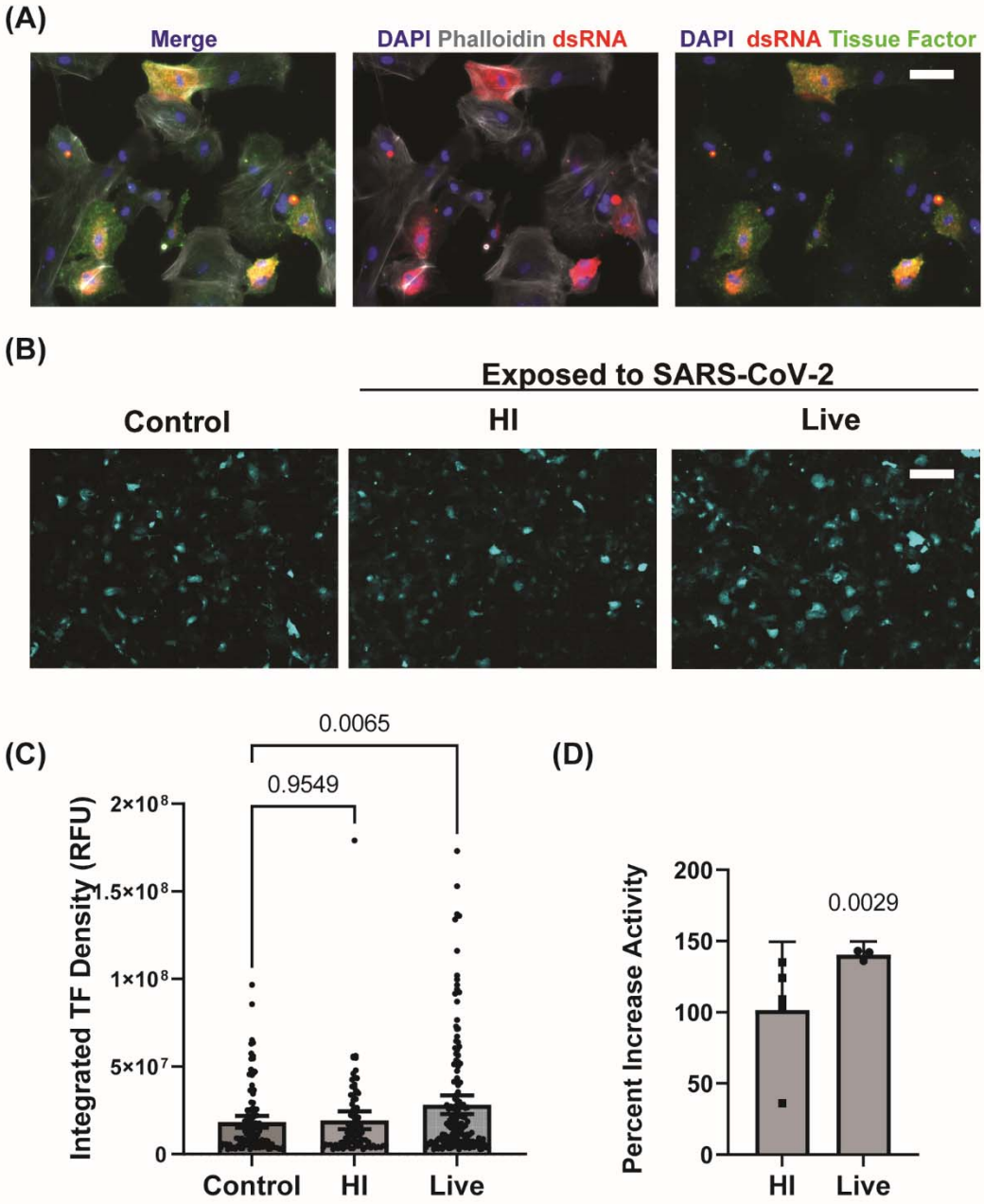

Figure 6: SARS-CoV-2 infection of hPSC-derived SMCs increases tissue factor expression and activity. (A) Immunofluorescence staining of SARS-CoV-2 infected SMCs for dsRNA and tissue factor. Staining of actin with phalloidin was included to mark cell bodies. Cells were fixed at 48 hours post-infection. **(B)** Immunofluorescence staining for tissue factor in hPSC-derived SMCs exposed to either live or heat-inactivated (HI) SARS-CoV-2 or uninfected control hPSC-derived SMCs. Cells were fixed at 48 hours post-infection. Scale bar = 200 µm (**C)** Quantitation of tissue factor staining shown in (A). **(D)**Tissue factor activity in cell lysate from SMCs exposed to live SARS-CoV-2 or HI SARS-CoV-2 was quantitated by ELISA and is reported as a percent increase compared to control uninfected SMCs.

Supplemental Figures:

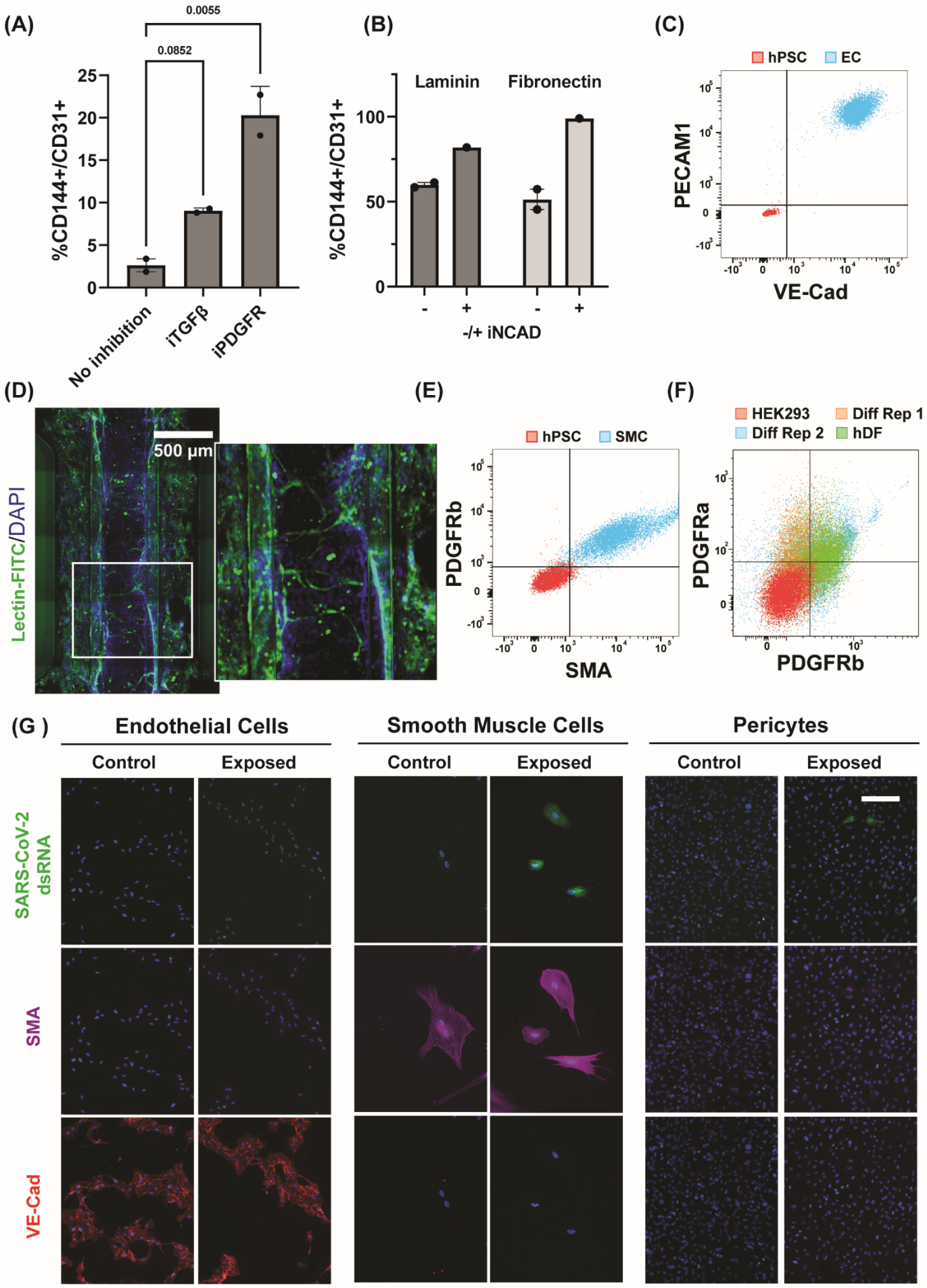
(A)
0.0055
0.0852
%CD144+/CD31+
No inhibition
iTGFβ
iPDGFR
(B)
Laminin
Fibronectin
%CD144+/CD31+
-/+ iNCAD
(C)
hPSC
EC
PECAM1
VE-Cad
(D)
500 µm
Lectin-FITC/DAPI
(E)
hPSC
SMC
PDGFRb
SMA
(F)
HEK293
Diff Rep 1
Diff Rep 2
hDF
PDGFRa
PDGFRb
(G)
Endothelial Cells
Smooth Muscle Cells
Pericytes
Control
Exposed
SARS-CoV-2 dsRNA
SMA
VE-Cad

Figure S1: Characterization and infection of hPSC-derived endothelial cells, pericytes, and smooth muscle cells. (A) Quantification of EC derivation efficiency by flow cytometry of double-positive PECAM1 and VE-Cad on two replicate differentiations with the dependence of either TGFβ or PDGFR inhibition. **(B)** Quantification of EC derivation efficiency by flow cytometry of double-positive PECAM1 and VE-Cad with the dependence of passaging on fibronectin or laminin and with or without N-cadherin inhibition (+/- iNCAD). **(C)** Representative flow cytometry dot plot of double-positive PECAM1 and VE-Cad expression after purification, expansion, cryopreservation, and thawing of hPSC-derived ECs. **(D)** Demonstration of angiogenic potential of hPSC-derived ECs in 3D microfluidic device after 48 hr of perfused culture. **(E)** Representative flow cytometry dot plot of double-positive PDGFRb and SMA expression after purification, expansion, cryopreservation, and thawing of hPSC-derived SMCs. **(F)** Representative flow cytometry dot plot of double-positive PDGFRb and PDGFRa expression after purification, expansion, cryopreservation, and thawing of hPSC-derived PCs. **(G)** Immunofluorescence staining for VE-cadherin, smooth muscle actin (SMA), and double-stranded RNA (dsRNA) 48 hours after exposure to SARS-CoV-2.

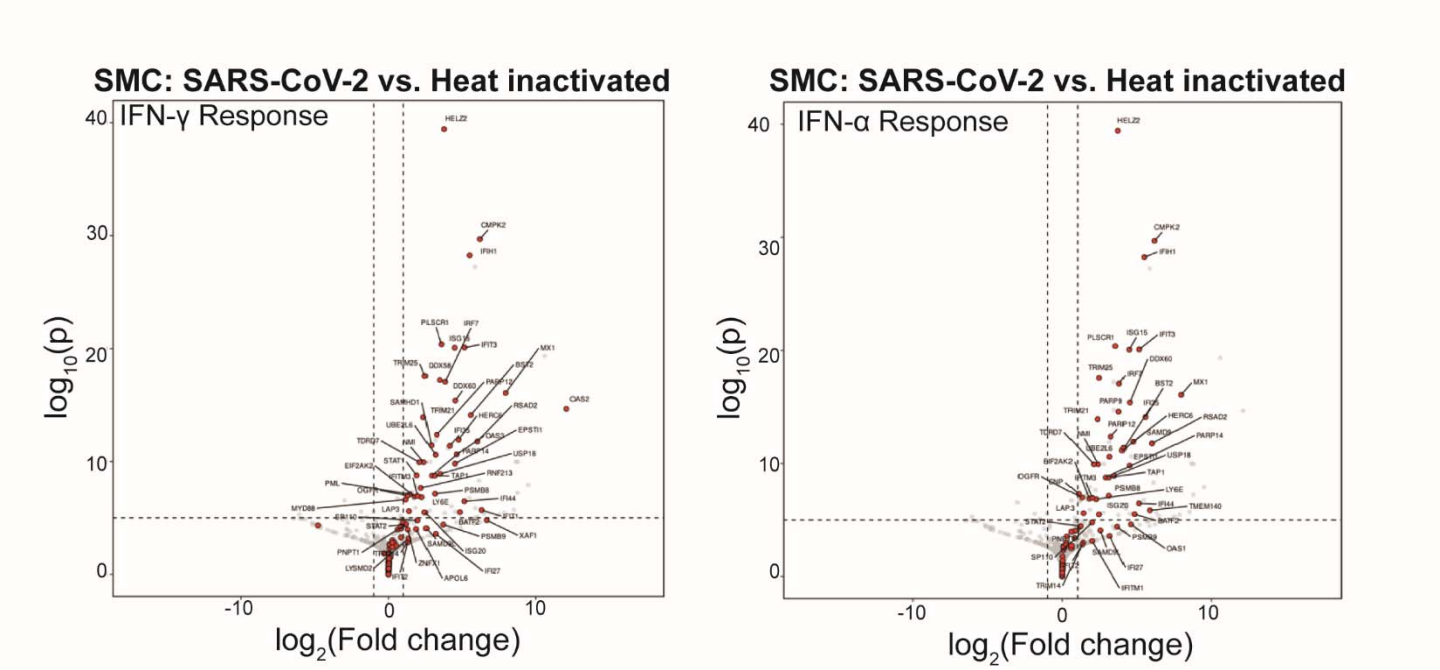

Figure S2: SARS-CoV-2 infection amplifies inflammatory signaling in SMCs.

Bulk RNA sequencing was performed on RNA isolated from hPSC-derived smooth muscle cells 48 hours after virus exposure (Figure 2B, 2D). The volcano plots show genes that are differentially expressed in SMCs exposed to live SARS-CoV-2 compared to SMCs exposed to heat-inactivated SARS-CoV-2 and highlight the "IFN-γ response" (left) and "IFN-α response" (right) gene-sets from the Hallmark collection[25] of the MSigDB. Genes that are highlighted in red belong to the respective interferon response gene-set, with GSEA "leading edge" genes labeled by name.

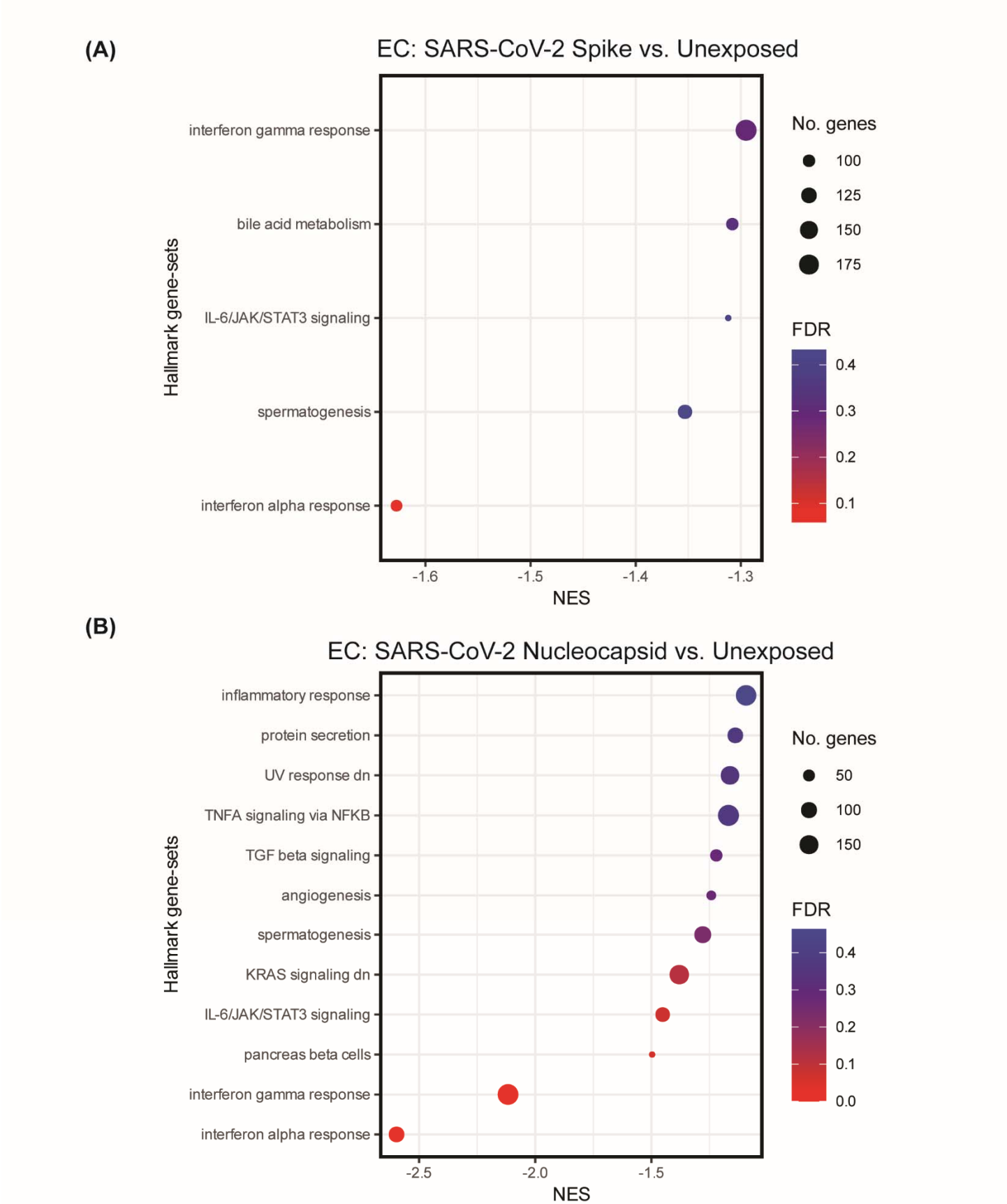

Figure S3: Gene expression changes in hPSC derived ECs following exposure to SARS-CoV-2 proteins. Bulk RNA sequencing was performed on RNA isolated from hPSC-derived vascular ECs 48 hours after exposing cells to purified SARS-CoV-2 proteins. Gene set enrichment analysis was

performed on sequenced bulk RNA samples collected. Dot plots show gene-sets from the Hallmark collection[25] Volcano plots showing differential gene expression in **(A)** ECs exposed to live SARS-CoV-2 compared to control uninfected ECs, **(B)** SMCs exposed to live SARS-CoV-2 compared to control uninfected SMCs.

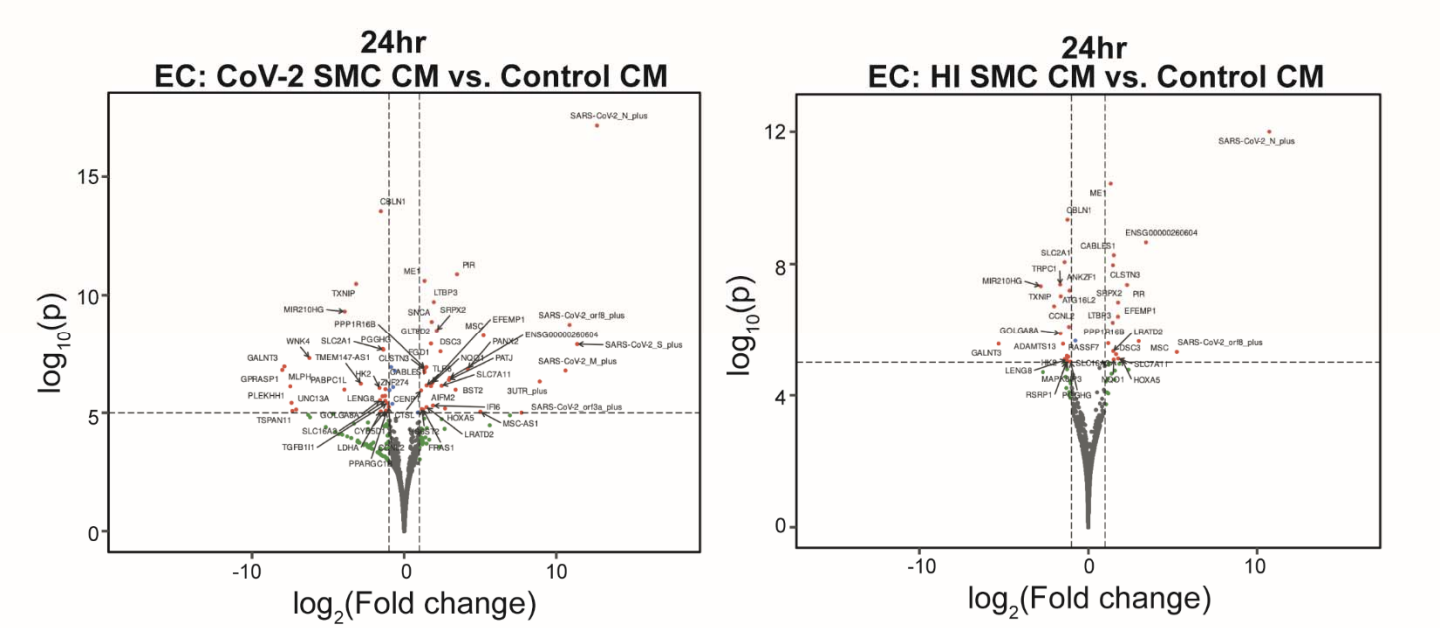

Figure S4: Early response of ECs to factors secreted from SARS-CoV-2 exposed SMCs: Bulk RNA sequencing was performed on RNA isolated from ECs 24 hours after exposure to SMC-conditioned media (Figure 4). The volcano plots show genes that are differentially expressed in **(A)** ECs exposed to media from SARS-CoV-2 infected SMCs (*CoV-2 SMC CM*) compared to ECs exposed to media from uninfected SMCs *(Control CM)* and **(B)** ECs exposed to media from SMCs exposed to heat-inactivated SARS-CoV-2 *(HI SMC CM)* compared to ECs exposed to media from uninfected SMCs *(Control CM)*.

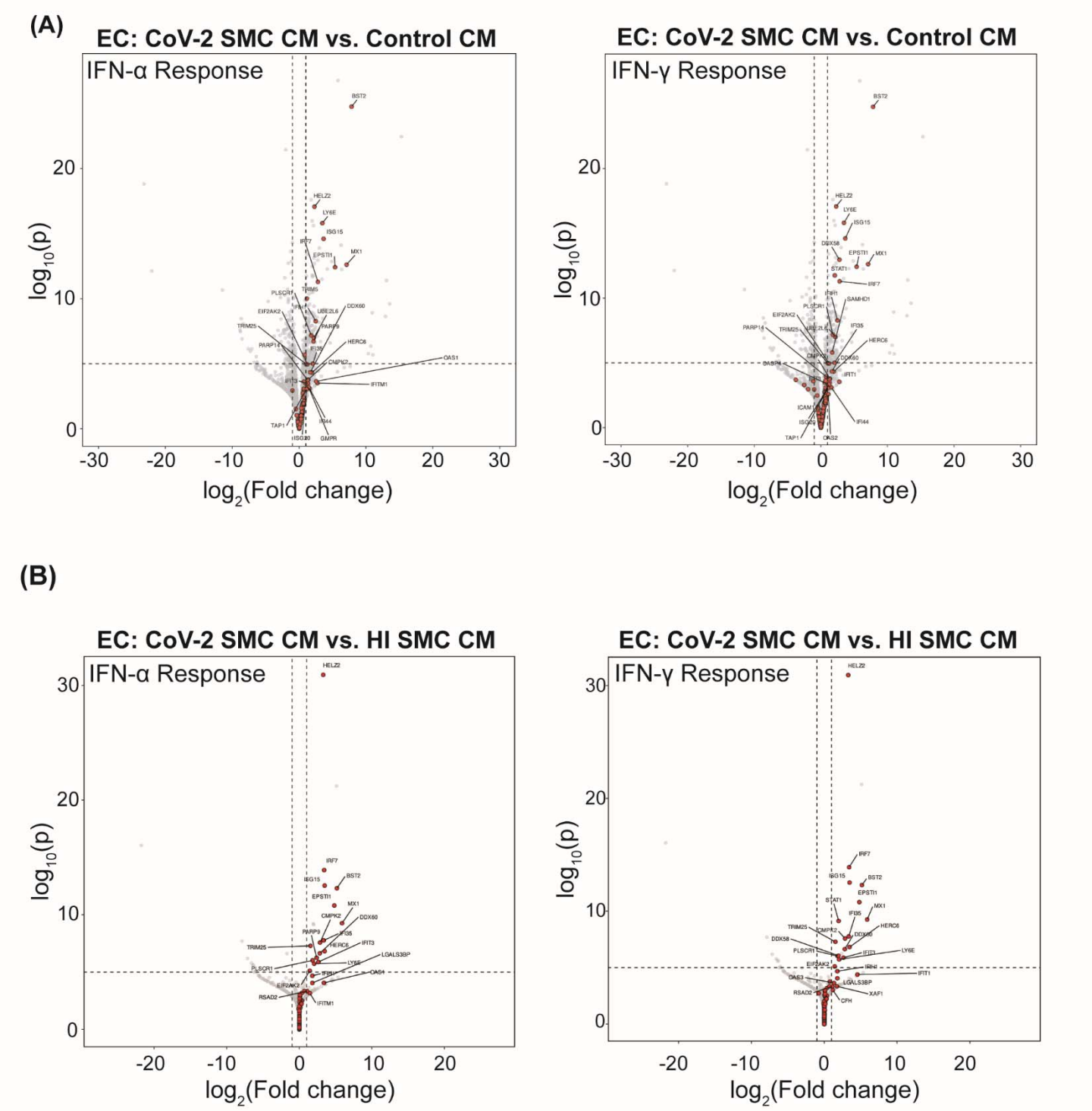

Figure S5: SARS-CoV-2 infected SMCs release factors that promote inflammatory signaling in ECs. Bulk RNA sequencing was performed on RNA isolated from ECs 48 hours after exposure to SMC-conditioned media **(**Figure 4). The volcano plots show genes that are differentially expressed in **(A)** ECs exposed to media from SARS-CoV-2 infected SMCs *(CoV-2 SMC CM)* compared to ECs exposed to media from uninfected SMCs *(Control CM)* and **(B)** ECs exposed to media from SARS-CoV-2 infected SMCs *(CoV-2 SMC CM)* compared to ECs exposed to media from SMCs treated with heat-inactivated SARS-CoV-2 *(HI SMC CM)*. In both comparisons genes from the "IFN-α response"

(left) and “IFN-γ response” (right) gene-sets of the MSigDB’s Hallmark collection[25] are highlighted in red, with GSEA “leading edge” genes indicated by name.

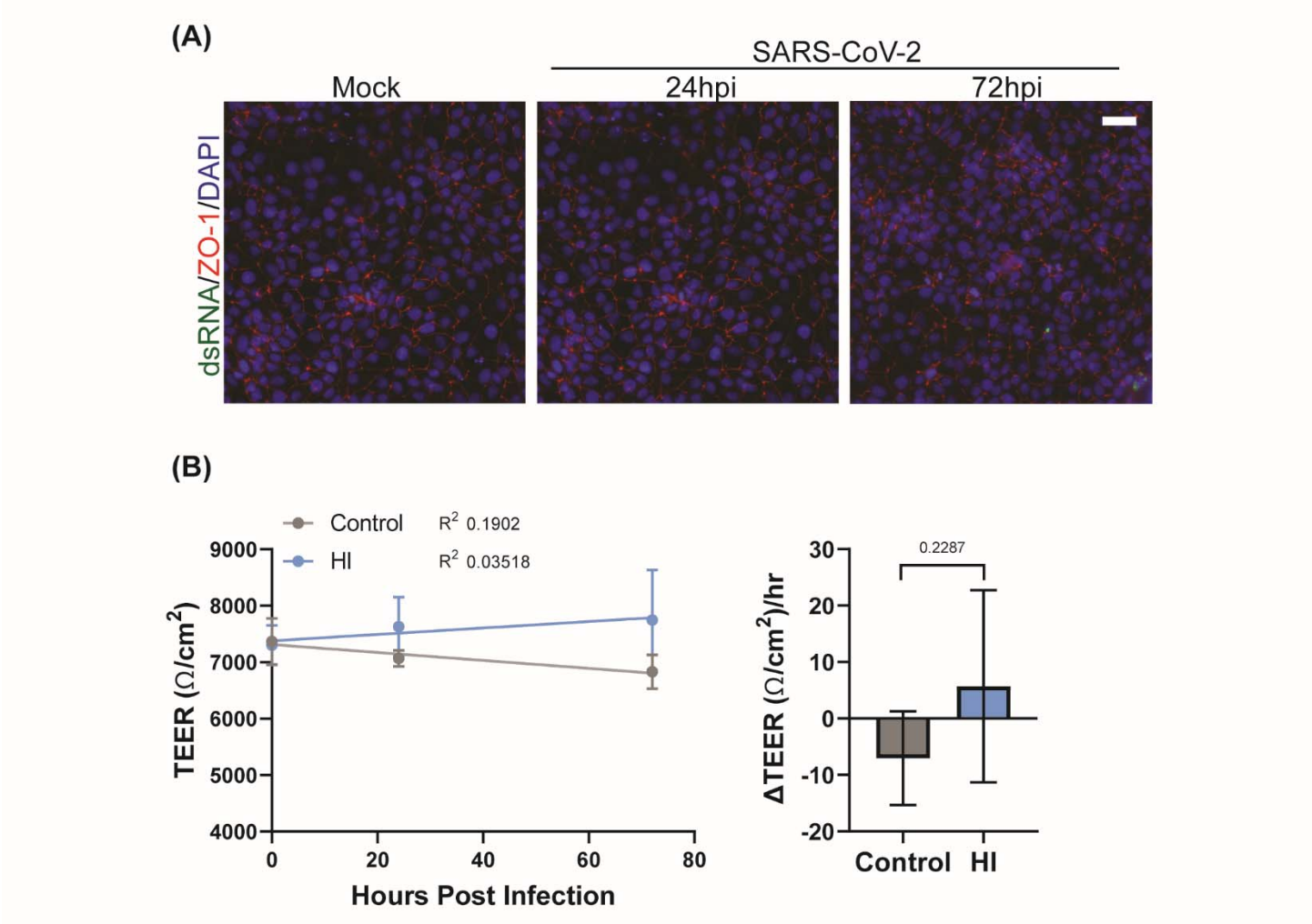

Figure S6: Exposure of hPSC-derived brain microvascular cells to SARS-CoV-2. (A) hPSC-derived brain microvascular endothelial cells (hBMECs) were exposed to live SARS-CoV-2 for 48 hours. Cells were fixed and stained for the tight junction marker ZO-1 and dsRNA to detect viral replication. **(B)** hBMECs were plated in trans-well plates and exposed to media from SMCs treated with heat-inactivated SARS-CoV-2 (HI) or media from uninfected SMCs (*Control)*. Trans-endothelial cell electrical resistance (TEER) was measured at 0, 24, and 72 hours after exposure.

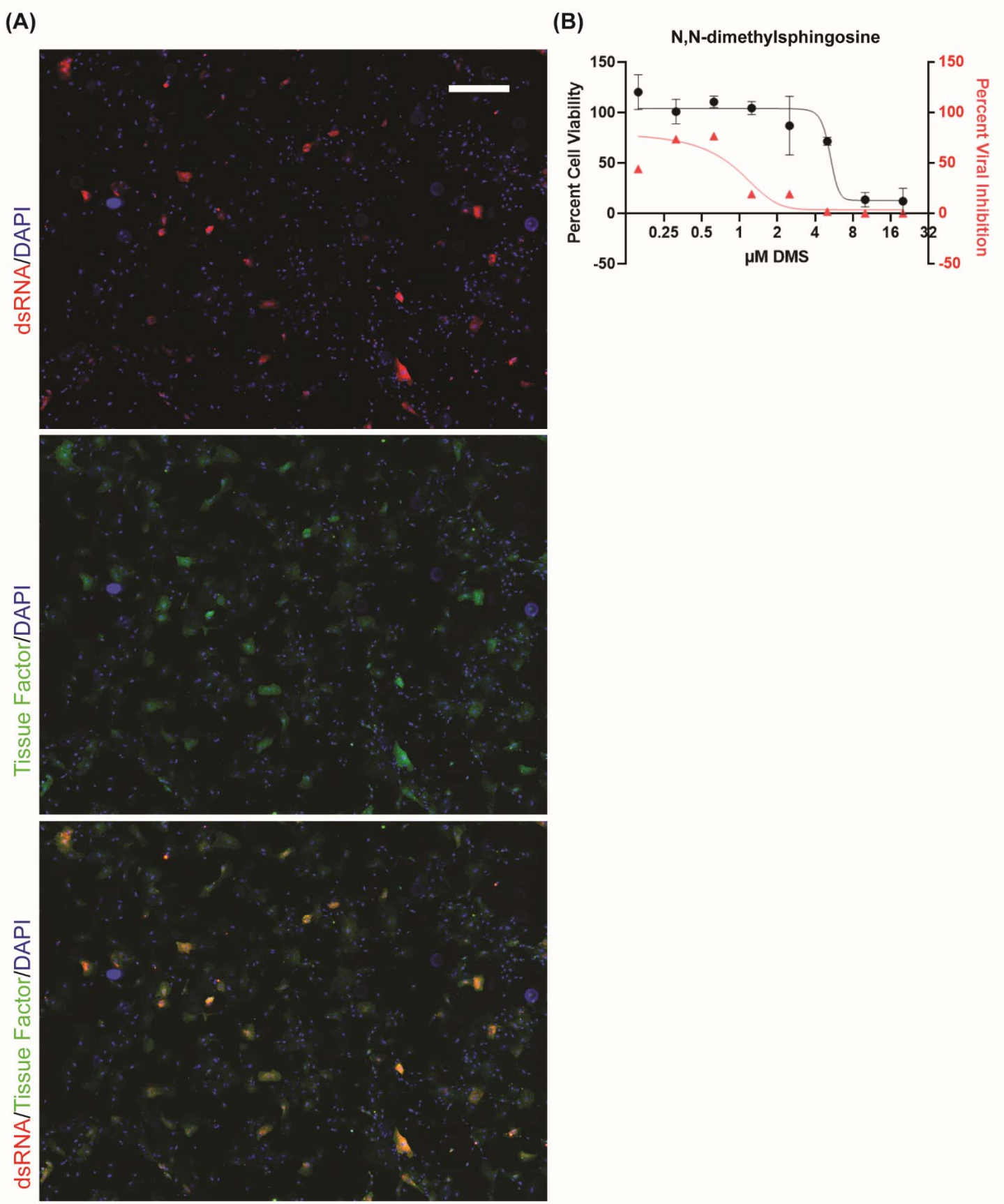

Figure S7: The SPHK inhibitor N,N-dimethyl-sphingosine reduces SARS-CoV-2 replication in hPSC-derived SMCs. (A) Representaive immunofluorescence micrograph showing association of TF expression in infected SMCs with the presence of the 15.78% (155/982 DAPI+ cells) dsRNA-positive

cells. Scale bar = 200 µm **(B)** SARS-CoV-2 infected SMCs were exposed to increasing amounts of N,N-dimethyl-sphingosine (DMS) during infection. The amount of infectious virus released into the media at 48 hours post-infection was quantitated by plaque assay. Cell viability was measured in uninfected SMCs at the corresponding time point and DMS dose.

Table 1

Primary Antibodies	Source	Catalog Number	Dilution
VE-Cadherin	R&D Systems	AF938	1:250
vWF	Abcam	ab6994	1:250
PECAM1(CD31)	Abcam	ab9498	1:250
SMA	Abcam	ab5694	1:200
PDGFRβ	Cell Signaling	3169S	1:200
NG2	Invitrogen	14-6504-82	1:200
dsRNA (J2)	Novus	NBP3-11395	1:2000
Tissue Factor	Abcam	ab228968	1:250
ZO-1	Life Technologies	402200	1:200
VE-Cadherin-PE (Flow for EC)	Invitrogen	12-1449-82	1:50
PECAM1-AlexaFluor 647 (Flow for EC)	Abcam	Ab215912	1:50
SMA-AlexaFluor 594 (Flow for SMC)	Cell Signaling	36110S	1:50
PDGFRb-APC (Flow for SMC)	Abcam	Ab119861	1:50
NG2-APC (Flow for PC)	R&D Systems	FAB2585A	1:25
PDGFRb-APC (Flow for PC)	BioLegend	323512	1:25
PDGFRa-PE (Flow for PC)	BioLegend	323606	1:25
Secondary Antibodies	Source	Catalog Number	Dilution
Mouse-488	Life Technologies	A21202	1:1000
Mouse-568	Life Technologies	A10037	1:1000
Mouse-647	Life Technologies	A31571	1:1000
Rabbit-488	Life Technologies	A21206	1:1000
Rabbit-568	Life Technologies	A11011	1:1000
Rabbit-647	Life Technologies	A31573	1:1000
Goat-488	Life Technologies	A11055	1:1000
Goat-568	Life Technologies	A11057	1:1000

Goat-647	Life Technologies	A21447	1:1000

Table 2

	Final Concentration	Source	Catalog #
MelM			
E6		Thermo Fisher Scientific	A1516401
L-Ascorbic acid 2-phosphate sesquimagnesium salt hydrate (AA)	60ug/ml	Sigma	A8960-5G
CHIR 99021	8uM	Biogems	2520691
BMP4	25ng/ml	Peprotech	120-05ET

	Final Concentration	Source	Catalog #
EC1			
E6		Thermo Fisher Scientific	A1516401
Forskolin	2nM	Biogems	6652995
AA	60ug/ml	Sigma	A8960-5G
VEGF	200ng/ml	Peprotech	100-20-50µg
CP-673451	2nM	Selleck	S1536
SB 431542	10uM	Biogems	3014193
EC2			
hESFM		Thermo Fisher Scientific	11111044
Forskolin	2nM	Biogems	6652995
AA	60ug/ml	Sigma	A8960-5G
VEGF	200ng/ml	Peprotech	100-20-50µg
CP-673451	2nM	Selleck	S1536
SB 431542	10uM	Biogems	3014193
EC3			
hESFM		Thermo Fisher Scientific	11111044
AA	60ug/ml	Sigma	A8960-5G
VEGF	200ng/ml	Peprotech	100-20-50µg
CP-673451	2nM	Selleck	S1536
SB 431542	10uM	Biogems	3014193
Exherin (ADH-1)	25ug/ml	AdooQ BioScience	A13689
EC4			
hESFM		Thermo Fisher Scientific	11111044
B27	1:50	Thermo Fisher Scientific	17504044
EGF	20ng/ml	Peprotech	AF-100-15
Heparin	2ug/ml	StemCell Technologies	07980
VEGF	20ng/ml	Peprotech	100-20-50µg
CP-673451	2nM	Selleck	S1536
SB 431542	10uM	Biogems	3014193
S1P	5nM	Sigma	S9666-1MG
EC5			
hESFM		Thermo Fisher Scientific	11111044
B27	1:50	Thermo Fisher Scientific	17504044
EGF	20ng/ml	Peprotech	AF-100-15
Heparin	2ug/ml	StemCell Technologies	07980
VEGF	20ng/ml	Peprotech	100-20-50µg
bFGF	50ng/ml	Peprotech	100-18B

	Final Concentration	Source	Catalog #
PC/SMC1			
E6		Thermo Fisher Scientific	A1516401
Forskolin	2nM	Biogems	6652995
AA	60ug/ml	Sigma	A8960-5G
VEGF	200ng/ml	Peprotech	100-20-50µg
PC2/SMC2			
hESFM		Thermo Fisher Scientific	11111044
Forskolin	2nM	Biogems	6652995
AA	60ug/ml	Sigma	A8960-5G
VEGF	200ng/ml	Peprotech	100-20-50µg
PC3			
hESFM		Thermo Fisher Scientific	11111044
AA	60ug/ml	Sigma	A8960-5G
VEGF	200ng/ml	Peprotech	100-20-50µg
SB 431542	10uM	Biogems	3014193
PC4			
hESFM		Thermo Fisher Scientific	11111044
B27	1:50	Thermo Fisher Scientific	17504044
EGF	20ng/ml	Peprotech	AF-100-15
Heparin	2ug/ml	StemCell Technologies	07980
SB 431542	10uM	Biogems	3014193
PDGFbb	10ng/ml	Peprotech	100-14B-10UG

	Final Concentration	Source	Catalog #
SMC3			
hESFM		Thermo Fisher Scientific	11111044
AA	60ug/ml	Sigma	A8960-5G
VEGF	200ng/ml	Peprotech	100-20-50µg
CP-673451	2nM	Selleck	S1536
SMC4			
hESFM		Thermo Fisher Scientific	11111044
B27	1:50	Thermo Fisher Scientific	17504044
EGF	20ng/ml	Peprotech	AF-100-15
Heparin	2ug/ml	StemCell Technologies	07980
CP-673451	2nM	Selleck	S1536
SMC5			
hESFM		Thermo Fisher Scientific	11111044
B27	1:50	Thermo Fisher Scientific	17504044
EGF	20ng/ml	Peprotech	AF-100-15
Heparin	2ug/ml	StemCell Technologies	07980
TGFβ	10ng/mlM	Peprotech	100-21-500ug

References

1. Spyropoulos, A.C. *et al.* Occurrence of Thromboembolic Events and Mortality Among Hospitalized Coronavirus 2019 Patients: Large Observational Cohort Study of Electronic Health Records. *TH Open* **6**, e408-e420 (2022).
2. Belani, P. *et al.* COVID-19 Is an Independent Risk Factor for Acute Ischemic Stroke. *AJNR Am J Neuroradiol* **41**, 1361-1364 (2020).
3. Arora, P., Jafferany, M., Lotti, T., Sadoughifar, R. & Goldust, M. Learning from history: Coronavirus outbreaks in the past. *Dermatol Ther* **33**, e13343 (2020).
4. WHO, Vol. 2021 (
5. Acharya, Y., Alameer, A., Calpin, G., Alkhattab, M. & Sultan, S. A comprehensive review of vascular complications in COVID-19. *J Thromb Thrombolysis* **53**, 586-593 (2022).
6. Merschel, M. in American Heart Association News Stories, Edn. February 24, 2023 (2023).
7. Xie, Y., Xu, E., Bowe, B. & Al-Aly, Z. Long-term cardiovascular outcomes of COVID-19. *Nat Med* **28**, 583-590 (2022).
8. Ackermann, M. *et al.* Pulmonary Vascular Endothelialitis, Thrombosis, and Angiogenesis in Covid-19. *N Engl J Med* **383**, 120-128 (2020).
9. Schimmel, L. *et al.* Endothelial cells are not productively infected by SARS-CoV-2. *Clin Transl Immunology* **10**, e1350 (2021).
10. Urata, R. *et al.* Senescent endothelial cells are predisposed to SARS-CoV-2 infection and subsequent endothelial dysfunction. *Sci Rep* **12**, 11855 (2022).
11. McQuaid, C. & Montagne, A. SARS-CoV-2 and vascular dysfunction: a growing role for pericytes. *Cardiovasc Res* (2022).
12. Stein, S.R. *et al.* SARS-CoV-2 infection and persistence in the human body and brain at autopsy. *Nature* **612**, 758-763 (2022).
13. Lilly, B. We have contact: endothelial cell-smooth muscle cell interactions. *Physiology (Bethesda)* **29**, 234-241 (2014).
14. Mendez-Barbero, N., Gutierrez-Munoz, C. & Blanco-Colio, L.M. Cellular Crosstalk between Endothelial and Smooth Muscle Cells in Vascular Wall Remodeling. *Int J Mol Sci* **22** (2021).
15. Patsch, C. *et al.* Generation of vascular endothelial and smooth muscle cells from human pluripotent stem cells. *Nat Cell Biol* **17**, 994-1003 (2015).
16. Kumar, A. *et al.* Specification and Diversification of Pericytes and Smooth Muscle Cells from Mesenchymoangioblasts. *Cell Rep* **19**, 1902-1916 (2017).
17. Cao, G. *et al.* How vascular smooth muscle cell phenotype switching contributes to vascular disease. *Cell Commun Signal* **20**, 180 (2022).
18. Wanjare, M., Kuo, F. & Gerecht, S. Derivation and maturation of synthetic and contractile vascular smooth muscle cells from human pluripotent stem cells. *Cardiovasc Res* **97**, 321-330 (2013).
19. Sola, I., Almazan, F., Zuniga, S. & Enjuanes, L. Continuous and Discontinuous RNA Synthesis in Coronaviruses. *Annu Rev Virol* **2**, 265-288 (2015).
20. Lei, Y. *et al.* SARS-CoV-2 Spike Protein Impairs Endothelial Function via Downregulation of ACE 2. *Circ Res* **128**, 1323-1326 (2021).
21. Loveday, E.K. *et al.* Effect of Inactivation Methods on SARS-CoV-2 Virion Protein and Structure. *Viruses* **13** (2021).
22. Subramanian, A. *et al.* Gene set enrichment analysis: a knowledge-based approach for interpreting genome-wide expression profiles. *Proc Natl Acad Sci U S A* **102**, 15545-15550 (2005).
23. Ma, J., Sanchez-Duffhues, G., Goumans, M.J. & Ten Dijke, P. TGF-beta-Induced Endothelial to Mesenchymal Transition in Disease and Tissue Engineering. *Front Cell Dev Biol* **8**, 260 (2020).
24. Cooley, B.C. *et al.* TGF-beta signaling mediates endothelial-to-mesenchymal transition (EndMT) during vein graft remodeling. *Sci Transl Med* **6**, 227ra234 (2014).

25. Liberzon, A. *et al.* The Molecular Signatures Database (MSigDB) hallmark gene set collection. *Cell Syst* **1**, 417-425 (2015).
26. Lopez-Castaneda, S. *et al.* Inflammatory and Prothrombotic Biomarkers Associated With the Severity of COVID-19 Infection. *Clin Appl Thromb Hemost* **27**, 1076029621999099 (2021).
27. Choudhary, S., Sharma, K. & Singh, P.K. Von Willebrand factor: A key glycoprotein involved in thrombo-inflammatory complications of COVID-19. *Chem Biol Interact* **348**, 109657 (2021).
28. Helms, J. *et al.* High risk of thrombosis in patients with severe SARS-CoV-2 infection: a multicenter prospective cohort study. *Intensive Care Med* **46**, 1089-1098 (2020).
29. Schmidbauer, M.L. *et al.* COVID-19 and Intracranial Hemorrhage: A Multicenter Case Series, Systematic Review and Pooled Analysis. *J Clin Med* **11** (2022).
30. Keep, R.F. *et al.* Blood-brain barrier function in intracerebral hemorrhage. *Acta Neurochir Suppl* **105**, 73-77 (2008).
31. Stebbins, M.J. *et al.* Differentiation and characterization of human pluripotent stem cell-derived brain microvascular endothelial cells. *Methods* **101**, 93-102 (2016).
32. Helms, H.C. *et al.* In vitro models of the blood-brain barrier: An overview of commonly used brain endothelial cell culture models and guidelines for their use. *J Cereb Blood Flow Metab* **36**, 862-890 (2016).
33. Yang, R.C. *et al.* SARS-CoV-2 productively infects human brain microvascular endothelial cells. *J Neuroinflammation* **19**, 149 (2022).
34. Daniels, B.P. & Klein, R.S. Knocking on Closed Doors: Host Interferons Dynamically Regulate Blood-Brain Barrier Function during Viral Infections of the Central Nervous System. *PLoS Pathog* **11**, e1005096 (2015).
35. Srinivasan, B. *et al.* TEER measurement techniques for in vitro barrier model systems. *J Lab Autom* **20**, 107-126 (2015).
36. Wang, L. *et al.* Vascular smooth muscle-derived tissue factor is critical for arterial thrombosis after ferric chloride-induced injury. *Blood* **113**, 705-713 (2009).
37. Nguyen, D., Jeon, H.M. & Lee, J. Tissue factor links inflammation, thrombosis, and senescence in COVID-19. *Sci Rep* **12**, 19842 (2022).
38. Subrahmanian, S. *et al.* Tissue factor upregulation is associated with SARS-CoV-2 in the lungs of COVID-19 patients. *J Thromb Haemost* **19**, 2268-2274 (2021).
39. Spiegel, S. & Milstien, S. The outs and the ins of sphingosine-1-phosphate in immunity. *Nat Rev Immunol* **11**, 403-415 (2011).
40. Yanagida, K. & Hla, T. Vascular and Immunobiology of the Circulatory Sphingosine 1-Phosphate Gradient. *Annu Rev Physiol* **79**, 67-91 (2017).
41. Schuchardt, M., Tolle, M., Prufer, J. & van der Giet, M. Pharmacological relevance and potential of sphingosine 1-phosphate in the vascular system. *Br J Pharmacol* **163**, 1140-1162 (2011).
42. McGowan, E.M., Haddadi, N., Nassif, N.T. & Lin, Y. Targeting the SphK-S1P-SIPR Pathway as a Potential Therapeutic Approach for COVID-19. *Int J Mol Sci* **21** (2020).
43. Li, Y. *et al.* SARS-CoV-2 induces double-stranded RNA-mediated innate immune responses in respiratory epithelial-derived cells and cardiomyocytes. *Proc Natl Acad Sci U S A* **118** (2021).
44. Girgis, S. *et al.* Evolution of naturally arising SARS-CoV-2 defective interfering particles. *Commun Biol* **5**, 1140 (2022).
45. Qian, T. *et al.* Directed differentiation of human pluripotent stem cells to blood-brain barrier endothelial cells. *Sci Adv* **3**, e1701679 (2017).
46. Neal, E.H. *et al.* A Simplified, Fully Defined Differentiation Scheme for Producing Blood-Brain Barrier Endothelial Cells from Human iPSCs. *Stem Cell Reports* **12**, 1380-1388 (2019).
47. Dobin, A. *et al.* STAR: ultrafast universal RNA-seq aligner. *Bioinformatics* **29**, 15-21 (2013).
48. Liao, Y., Smyth, G.K. & Shi, W. featureCounts: an efficient general purpose program for assigning sequence reads to genomic features. *Bioinformatics* **30**, 923-930 (2014).
49. Love, M.I., Huber, W. & Anders, S. Moderated estimation of fold change and dispersion for RNA-seq data with DESeq2. *Genome Biol* **15**, 550 (2014).
50. Stephens, M. False discovery rates: a new deal. *Biostatistics* **18**, 275-294 (2017).